

**DEVELOPMENT AND EVALUATION OF  
FIBER OPTIC SENSORS**

**Final Report**

**PROJECT 312**



**DEVELOPMENT AND EVALUATION OF FIBER OPTIC  
SENSORS**

**Final Report**

**PROJECT 312**

by

Eric Udd  
and  
Marley Kunzler  
Blue Road Research  
276 NE 219<sup>th</sup> Avenue  
Gresham, Oregon 97030

for

Oregon Department of Transportation  
Research Group  
200 Hawthorne SE, Suite B-240  
Salem OR 97301-5192

and

Federal Highway Administration  
Washington, D.C.

**May 2003**



1. Report No. FHWA-OR-RD-03-14		2. Government Accession No.		3. Recipient's Catalog No.	
4. Title and Subtitle Development and Evaluation of Fiber Optic Sensors				Report Date May 2003	
				Performing Organization Code	
7. Author(s) Eric Udd and Marley Kunzler				8. Performing Organization Report No.	
9. Performing Organization Name and Address  Blue Road Research 376 NE 219 <sup>th</sup> Avenue Gresham, Oregon 97030				10. Work Unit No. (TRAIS)	
				Contract or Grant No.  SPR 312	
12. Sponsoring Agency Name and Address  Oregon Department of Transportation Research Group and Federal Highway Administration 200 Hawthorne SE, Suite B-240 Washington, D.C. Salem, Oregon 97301-5192				13. Type of Report and Period Covered  Final Report	
				14. Sponsoring Agency Code	
15. Supplementary Notes					
16. Abstract  <p>This study investigated the feasibility of using fiber optic sensors to capture traffic data. Funding from the study was used to develop a prototype sensor using fiber Bragg gratings (FBG) technology. The sensor was tested on a high volume portland cement concrete highway and found to be feasible for use in monitoring light and heavy traffic. Signals from the sensor were processed with a demodulator system, and captured on a computer. For testing purposes, the signal was converted to a scaled analog voltage signal and successfully output to a conventional traffic classifier recorder.</p> <p>The sensors have the potential for long-lasting, cost-effective solutions in vehicle classification applications. With modification, the FBG strain sensor shows potential for use in weigh-in-motion applications.</p> <p>The system is sensitive enough to detect adjacent lane traffic, opening possibilities of shoulder area monitoring for less traffic disruption and increased safety. With two sensors, the system can capture speeds as well as weights of both sides of a vehicle.</p> <p>Future development of dedicated demodulator/interfacing electronic hardware and auto-tuning grating system could eventually lead to cost effective solutions for traffic classification and weigh-in-motion applications.</p>					
17. Key Words Traffic monitoring, vehicle classification, fiber optic sensors, fiber Bragg gratings, weigh in motion			18. Distribution Statement Copies available from NTIS, and online at <a href="http://www.odot.state.or.us/tddresearch">http://www.odot.state.or.us/tddresearch</a>		
19. Security Classification (of this report) Unclassified		Security Classification (of this page) Unclassified		21. No. of Pages	22. Price

## SI\* (MODERN METRIC) CONVERSION FACTORS

### APPROXIMATE CONVERSIONS TO SI UNITS

Symbol	When You Know	Multiply By	To Find	Symbol
<b><u>LENGTH</u></b>				
in	inches	25.4	millimeters	mm
ft	feet	0.305	meters	m
yd	yards	0.914	meters	m
mi	miles	1.61	kilometers	km
<b><u>AREA</u></b>				
in <sup>2</sup>	square inches	645.2	millimeters squared	mm <sup>2</sup>
ft <sup>2</sup>	square feet	0.093	meters squared	m <sup>2</sup>
yd <sup>2</sup>	square yards	0.836	meters squared	m <sup>2</sup>
ac	acres	0.405	hectares	ha
mi <sup>2</sup>	square miles	2.59	kilometers squared	km <sup>2</sup>
<b><u>VOLUME</u></b>				
fl oz	fluid ounces	29.57	milliliters	ml
gal	gallons	3.785	liters	L
ft <sup>3</sup>	cubic feet	0.028	meters cubed	m <sup>3</sup>
yd <sup>3</sup>	cubic yards	0.765	meters cubed	m <sup>3</sup>
NOTE: Volumes greater than 1000 L shall be shown in m <sup>3</sup> .				
<b><u>MASS</u></b>				
oz	ounces	28.35	grams	g
lb	pounds	0.454	kilograms	kg
T	short tons (2000 lb)	0.907	megagrams	Mg
<b><u>TEMPERATURE (exact)</u></b>				
°F	Fahrenheit	(F-32)/1.8	Celsius	°C

### APPROXIMATE CONVERSIONS FROM SI UNITS

Symbol	When You Know	Multiply By	To Find	Symbol
<b><u>LENGTH</u></b>				
mm	millimeters	0.039	inches	in
m	meters	3.28	feet	ft
m	meters	1.09	yards	yd
km	kilometers	0.621	miles	mi
<b><u>AREA</u></b>				
mm <sup>2</sup>	millimeters squared	0.0016	square inches	in <sup>2</sup>
m <sup>2</sup>	meters squared	10.764	square feet	ft <sup>2</sup>
m <sup>2</sup>	meters squared	1.196	square yards	yd <sup>2</sup>
ha	hectares	2.47	acres	ac
km <sup>2</sup>	kilometers squared	0.386	square miles	mi <sup>2</sup>
<b><u>VOLUME</u></b>				
ml	milliliters	0.034	fluid ounces	fl oz
L	liters	0.264	gallons	gal
m <sup>3</sup>	meters cubed	35.315	cubic feet	ft <sup>3</sup>
m <sup>3</sup>	meters cubed	1.308	cubic yards	yd <sup>3</sup>
<b><u>MASS</u></b>				
g	grams	0.035	ounces	oz
kg	kilograms	2.205	pounds	lb
Mg	megagrams	1.102	short tons (2000 lb)	T
<b><u>TEMPERATURE (exact)</u></b>				
°C	Celsius	1.8C+32	Fahrenheit	°F

\*SI is the symbol for the International System of Measurement

## **DISCLAIMER**

This document is disseminated under the sponsorship of the Oregon Department of Transportation and the United States Department of Transportation in the interest of information exchange. The State of Oregon and the United States Government assume no liability of its contents or use thereof.

The contents of this report reflect the view of the authors who are solely responsible for the facts and accuracy of the material presented. The contents do not necessarily reflect the official views of the Oregon Department of Transportation or the United States Department of Transportation.

The State of Oregon and the United States Government do not endorse products of manufacturers. Trademarks or manufacturers' names appear herein only because they are considered essential to the object of this document.

This report does not constitute a standard, specification, or regulation.



# DEVELOPMENT AND EVALUATION OF FIBER OPTIC SENSORS

## TABLE OF CONTENTS

<b>1.0</b>	<b>INTRODUCTION.....</b>	<b>1</b>
1.1	FBG TRAFFIC SENSOR ADVANTAGES .....	1
1.2	THEORY OF OPERATION FOR FBG TRAFFIC SENSOR PROTOTYPES.....	2
<b>2.0</b>	<b>VEHICLE MONITORING TEST PAD.....</b>	<b>7</b>
2.1	INSTALLATION OF TEST PAD AND FBG TRAFFIC SENSORS .....	7
2.2	DATA OBTAINED FROM THE TEST PAD .....	10
2.2.1	<i>AC Response on the Test Pad</i> .....	10
2.2.2	<i>PCC Response on the Test Pad</i> .....	11
2.3	CONCLUSIONS FROM TEST PAD STUDY .....	11
<b>3.0</b>	<b>TESTING PROTOTYPE FBG TRAFFIC SENSORS.....</b>	<b>13</b>
3.1	INSTALLATION OF THE FBG TRAFFIC SENSOR IN THE INTERSTATE 84 FREEWAY WESTBOUND LANE .....	13
3.2	DATA OBTAINED FROM THE I-84 FREEWAY.....	16
3.2.1	<i>Evaluation of the Sensors Placed in the I-84 Freeway</i> .....	16
3.2.2	<i>Sensor Response and Durability</i> .....	17
3.3	RESULTS OF INTERSTATE 84 MONITORING .....	20
<b>4.0</b>	<b>REDESIGNING THE FBG TRAFFIC SENSORS .....</b>	<b>23</b>
4.1	CONSIDERATION FOR A REDESIGNED SENSOR.....	23
4.2	REVIEW OF PROPOSED DESIGNS.....	24
4.3	FREEWAY LAYOUT AND MANUFACTURING.....	26
4.3.1	<i>Manufacture &amp; Installation of FBG Traffic Sensors</i> .....	26
4.4	EVALUATION OF REDESIGNED FIBER OPTIC SENSORS .....	30
<b>5.0</b>	<b>INTERFACING THE FIBER OPTIC TRAFFIC SENSORS FOR VEHICLE CLASSIFICATION .....</b>	<b>35</b>
<b>6.0</b>	<b>A LOOK AT REMNANTS OF AN ORIGINAL TRAFFIC SENSOR.....</b>	<b>37</b>
<b>7.0</b>	<b>CONCLUSIONS .....</b>	<b>41</b>
<b>8.0</b>	<b>EVALUATION AND RECOMMENDATIONS .....</b>	<b>43</b>
<b>9.0</b>	<b>FUTURE WORK .....</b>	<b>45</b>
<b>10.0</b>	<b>REFERENCES.....</b>	<b>47</b>

## LIST OF TABLES

Table 2.1: Sensor installation variables for the vehicle test pad.....	8
Table 3.1: FBG sensor layout.....	15
Table 3.2: Chart showing spectral values (in nm) for the traffic sensors.....	17
Table 4.1: The configuration of the second-generation fiber optic traffic sensors.....	26
Table 4.2: Wavelengths (in nm) of each second-generation sensor.....	33
Table 5.1: Standard data output by the Diamond Phoenix Traffic Classifier interfaced with FBG traffic sensors....	35

## LIST OF FIGURES

Figure 1.1: Data collected at the Horsetail Falls Bridge showing various profiles: A minivan, a small SUV, a small car, a man running, a man jumping 5 times, and a man walking on the bridge.....	2
Figure 1.2: Schematic for FBG traffic sensor and demodulation system.....	3
Figure 1.3: Fiber grating written onto core of fiber.....	3
Figure 1.4: Transmission and reflection spectra from fiber Bragg grating.....	4
Figure 1.5: A larger grating spacing will result in a reflected peak with higher center wavelength.....	4
Figure 1.1: Layout of traffic test pad and sensor system.....	7
Figure 2.2: The ½" width housing chosen for FBG traffic sensor tests.....	8
Figure 2.3: A 1/16" sensor shown with the anchor.....	8
Figure 2.4: Cutting slots for the FBG traffic sensor installation.....	9
Figure 2.5: Optimizing sensor channels for ideal fit prior to installation. Heater boxes were used for curing.....	9
Figure 2.6: Placing the ½" sensors into the AC test pad.....	9
Figure 2.7: Hot bituminous sealant was used to fill the channels for half of the sensors. The protruding mound was later removed so the surface can be completely level.....	9
Figure 2.8: AC test pad and PCC test pad after the traffic sensors were installed and sealants dried.....	10
Figure 2.9: Sensor response to a vehicle backing across the sensor.....	10
Figure 3.1: Site map of the final layout for FBG sensors.....	13
Figure 3.2: Layout of FBG traffic sensors on the westbound lane of I-84 freeway.....	14
Figure 3.3: Saw cuts were made into the freeway in a fan-out pattern.....	15
Figure 3.4: Trench for the fiber backbone carrying the traffic signals to a remote readout facility.....	15
Figure 3.5: Marking was placed for the saw cut.....	15
Figure 3.6: Sensors were placed into the freeway.....	15
Figure 3.7: The sensors can be seen as they were routed through the junction point and then fan out to their respective locations in the AC. The junction point and sawed channels were later filled with hot bituminous sealant.....	16
Figure 3.8: The ground-level junction box as it was prepared for protecting the connections between the freeway sensors and the fiber line. Right, an overview of the sensor area and the junction box.....	16
Figure 3.9: Left, semi-tractor trailer crossing embedded FBG sensors, traveling left to right. Response from two FBG sensors. From this data, velocity (57 mph), axle spacing and potentially weight may be determined.....	18
Figure 3.10: Data capture from a vehicle traveling 55 mph with 2.74 ft axle spacing.....	19
Figure 3.11: Profile of a small vehicle traveling 61 mph with 9.5 ft axle spacing.....	19
Figure 3.12: A Geo Metro and its profile are shown above. The graph shows relative amplitude versus time in seconds.....	20
Figure 3.13: A series of vehicles detected in the adjacent lane.....	20

Figure 4.1: Possible physically-damaged areas in sensor housing .....	24
Figure 4.2: A composite beam encloses a long-gage traffic sensor.....	24
Figure 4.3: Possible sensor redesign using a spring to dampen strain.....	25
Figure 4.4: Design for composite reinforcement of optical traffic sensors .....	26
Figure 4.5: Sensor layout and placement for second installation .....	27
Figure 4.6: Enhanced FBG traffic sensors used in the I-84 freeway (Sensor 6) .....	28
Figure 4.7: Long-gage composite FBG traffic sensors (LGC) configuration. The composite beam provides rigid support to prevent overstrain.....	28
Figure 4.8: A composite sensor after being placed in the saw cut, awaiting bituminous sealant to complete the installation.....	29
Figure 4.9: The sensor after one pass of bituminous sealant is applied.....	29
Figure 4.10: Responsiveness is tested by jumping a few times near each sensor .....	30
Figure 4.11: The LGE (first peak/dotted line) and LGC sensors, respectively, react to a 5-axle vehicle .....	31
Figure 4.12: The LGE sensor (first peak/dotted line) appears to recover slightly faster than the LGC sensor.....	31
Figure 4.13: The LGC (lighter dashed line) and the UNC sensor react to traffic passing over .....	32
Figure 4.14: The LGC (lighter dashed line) and the UNC sensor react to traffic. The UNC appears to recover slightly faster.....	32
Figure 4.15: Two identical LGC sensors profile a vehicle. A baseline offset occurs in one line.....	33
Figure 5.1: The vehicle classifier box used to interface to the fiber optic sensors .....	35
Figure 6.1: A sensor lead extends from an extracted fiber optic sensor .....	37
Figure 6.2: Over-capacity local strain forces most likely caused this tubing to stretch apart, as found at the bottom of the saw cut.....	38
Figure 6.3: A 3 cm air pocket formed around this interface on the active sensing portion of the sensor.....	38
Figure 6.4: An arched sensor configuration is seen in this portion of the extraction .....	39



## 1.0 INTRODUCTION

Common vehicle detection sensors in civil applications use magnetometers, piezoelectric sensors, induction loops, video cameras, microwave devices and pneumatic rubber hoses, for a range of vehicle monitoring capabilities. They are used to count, classify and detect vehicles, monitor speed, and provide weigh-in-motion (WIM) data. The vehicle data captured by these devices is also used to forecast and plan transportation needs.

Although each specific device has advantages, its limiting characteristics require the use of various sensor types and suites to collect data for multiple areas of study. Additionally, the procedure for installation and the range of durability among these devices vary significantly.

The objectives of this study were to develop a working traffic sensor system with the potential to be more durable, reliable, and cost-effective than currently available traffic sensors, with a primary focus to design a sensor for vehicle counter and classifier applications. Other traffic sensing applications were to be investigated as time and funding permit.

### 1.1 FBG TRAFFIC SENSOR ADVANTAGES

Previous research done by Blue Road Research and the Oregon Department of Transportation (ODOT) has shown the capability of using fiber Bragg gratings (FBG) technology to monitor components of strain on bridges and structures, such as the Horsetail Falls Bridge in the Columbia River Gorge Scenic Area east of Portland. Data collected at that site strongly suggest that FBG strain sensors have the ability to monitor vehicle traffic (see Figure 1.1).

Using the reflected optical signals from FBGs, fiber sensors are capable of demodulation rates of hundreds to thousands of hertz. These rates are necessary to detect vehicle traffic ranging from quasi-static to freeway speeds. FBG technology and costs are improving due to close synergy with developments in the telecommunication industry (the leading force in component cost reduction).

One of the desired outcomes of the FBG traffic sensor is the ability to consolidate multiple conventional traffic sensor systems into one suite of nearly identical FBG traffic sensors. The FBG sensor has the capability of detecting many physical characteristics on or within the road. A future goal of the FBG traffic sensor is to consolidate multiple traffic and road measuring sensors into one package. A single FBG package could potentially provide simultaneous monitoring for weigh-in-motion, vehicle speed, classification, road fatigue, temperature, traffic signal vehicle detection and other traffic, road, and environmental characteristics. This provides several advantages including uniform and extended system durability, driver safety (*Meller et al 1998*), as well as simplified and cross-compatible traffic systems and data collection.

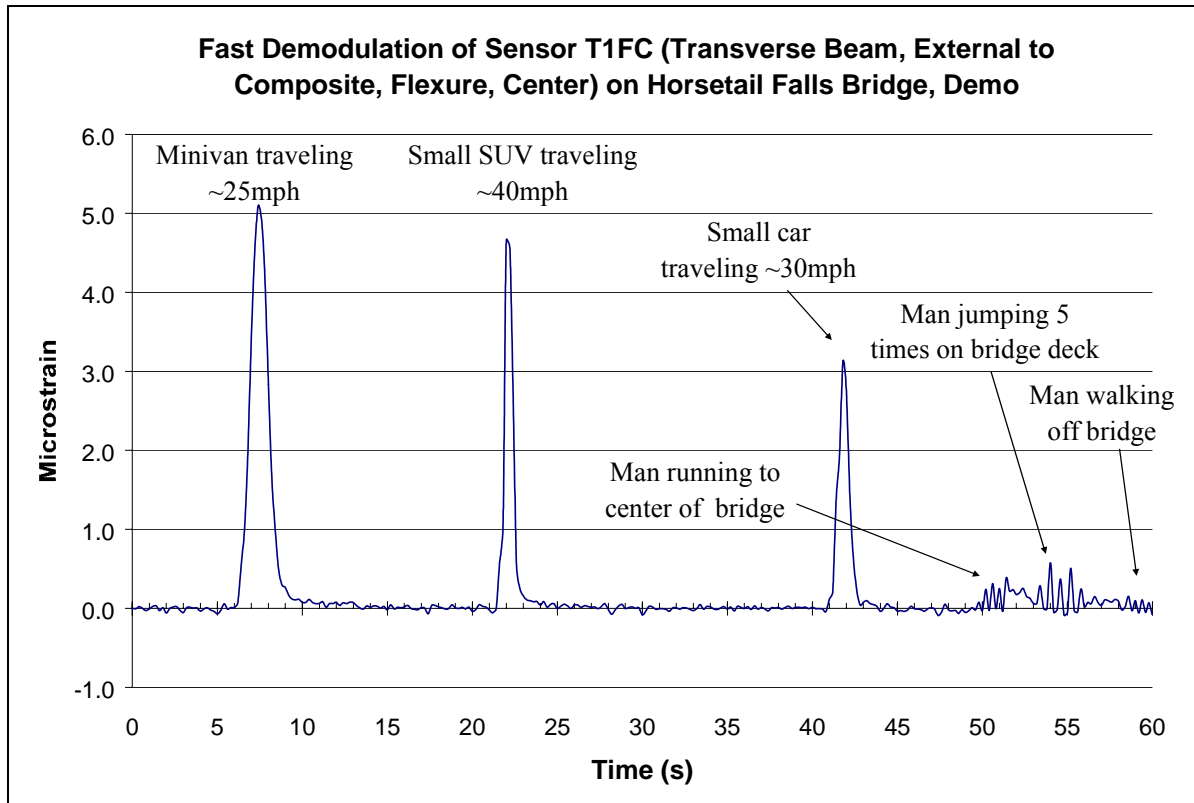


Figure 1.1: Data collected at the Horsetail Falls Bridge showing various profiles: A minivan, a small SUV, a small car, a man running, a man jumping 5 times, and a man walking on the bridge

The FBG traffic sensors hold all of the traditional advantages of fiber optics, including electrical isolation and increased bandwidth. They also have the ability to transmit over many miles with low signal loss, to be deployable in remote areas without electricity, to employ small size and weight, and to be immune to radio and electrical interference (unlike induction loops installed in steel-reinforced roadways). The FBG traffic sensors developed under this program are compatible with a family of sensors for roadway and civil applications, including humidity, ice, temperature, corrosion, and moisture sensors. Therefore, these traffic sensors can be integrated into an optical sensor system suite designed to monitor traffic, roadway, and weather conditions, improving safety factors along roadways and bridges.

Another aspect of the FBG sensors is that the demodulation system is external to the sensor. As the FBG traffic demodulation systems improve in accuracy and performance over time, the sensor system can undergo upgrades in sensitivity and accuracy without being removed from the roadway.

## 1.2 THEORY OF OPERATION FOR FBG TRAFFIC SENSOR PROTOTYPES

Using research and experience from previous bridge studies (*Schulz et al. 1999, Seim et al. 1999a, Seim et al. 1999b, Schulz et al. 1998, Udd et al. 2000*), Blue Road Research began to study and develop an FBG traffic sensor in the fall of 1999. These sensors were fabricated in

such a way that strain induced on road surfaces from vehicle weight is transferred into the FBG traffic sensor housings, straining the sensors in proportion to the vehicle weight and speed.

As shown in Figure 1.2, the system functions by using a broadband light source (BBS) channeled into a fiber optic strand approximately 155 microns in diameter with a polyimide coating. The BBS light couples through a beam splitter and illuminates a Bragg grating connected through fiber at a remote location.

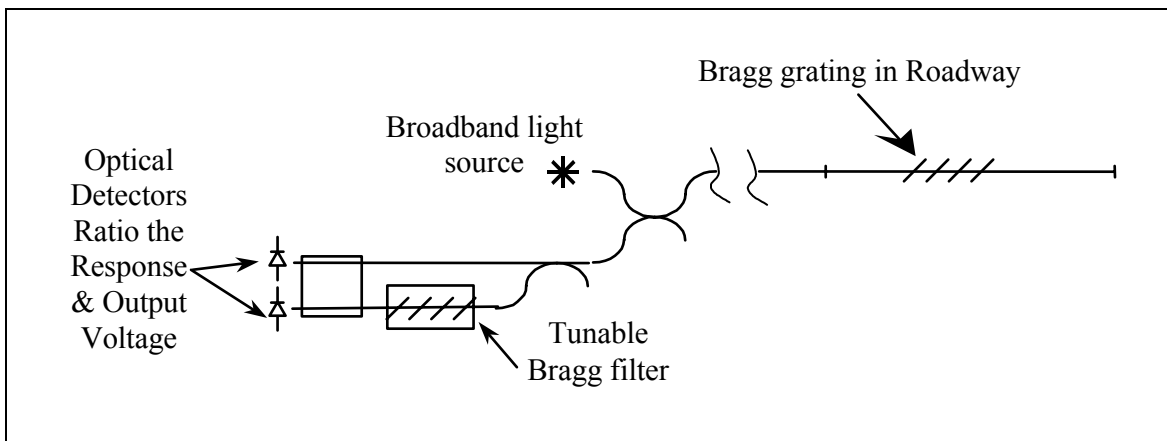


Figure 1.2: Schematic for FBG traffic sensor and demodulation system

Fiber gratings are formed by a periodic perturbation in the index of refraction along the length of the fiber. This grating, written onto the core of the optical fiber, has spacing “d” (Figure 1.3).

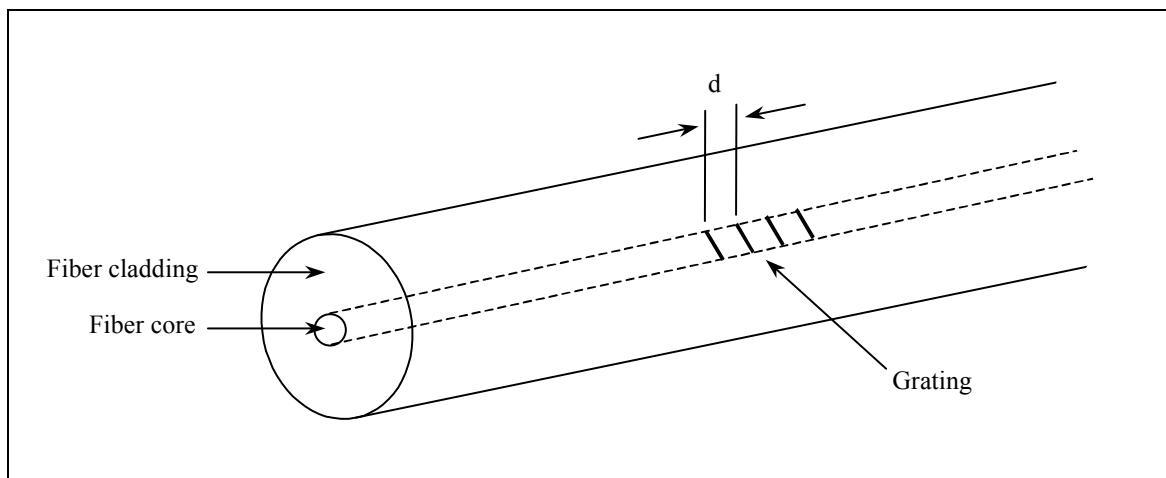


Figure 1.3: Fiber grating written onto core of fiber

This grating acts as a spectral filter and reflects a peak based on the grating spacing (Figure 1.4). The grating spacing affects the center wavelength of the reflected peak. A larger grating spacing results in higher wavelength reflections (Figure 1.5).

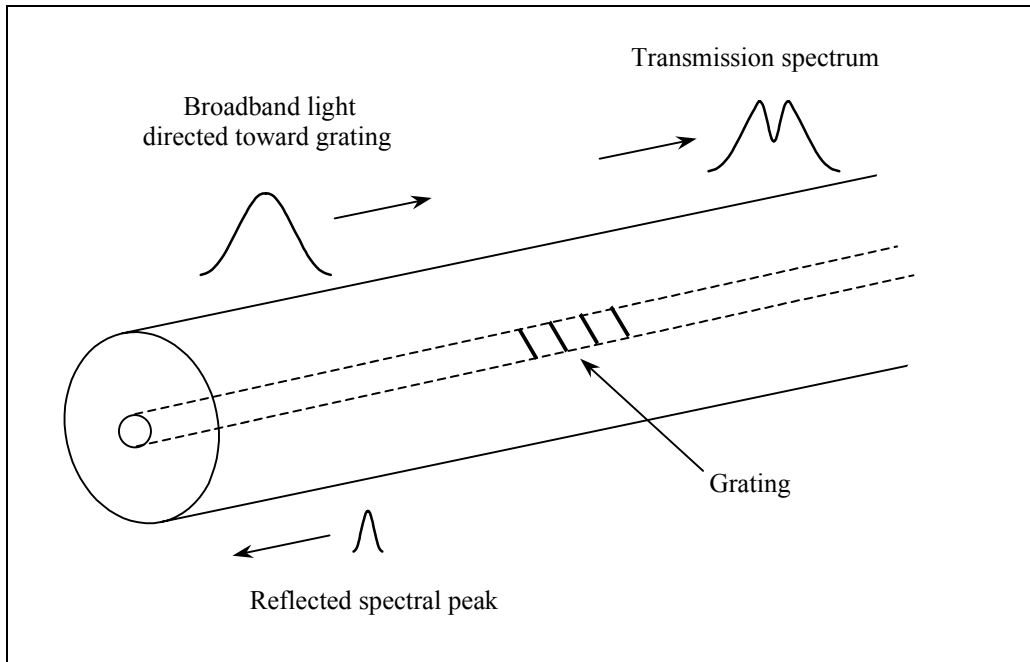


Figure 1.4: Transmission and reflection spectra from fiber Bragg grating

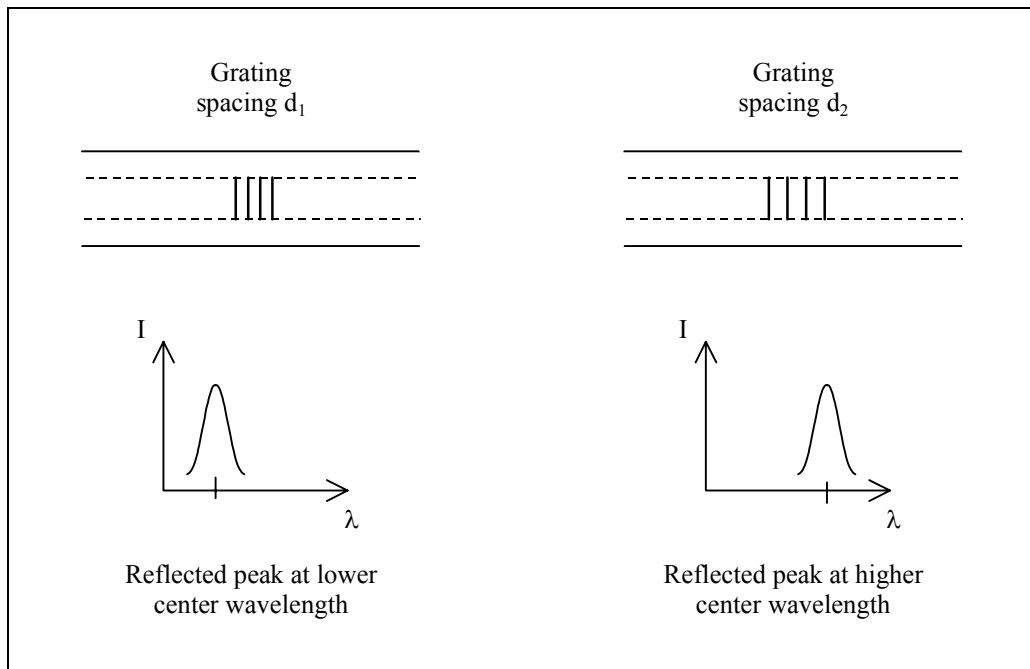


Figure 1.5: A larger grating spacing will result in a reflected peak with higher center wavelength

This relationship between grating spacing and reflected spectral peaks provides the capability to quantitatively measure strain along the fiber. This relationship is known as the Bragg equation:

$$\lambda = 2 \cdot d \cdot n \quad (1-1)$$

where:  $\lambda$  = center wavelength of reflected peak  
 $d$  = grating period  
 $n$  = index of refraction

Equation 1-1 can be manipulated to relate changes in the reflected wavelength as the fiber grating is stretched:

$$\Delta\lambda = 2 \cdot (\Delta d \cdot n + d \cdot \Delta n) \quad (1-2)$$

where:  $\Delta\lambda$  = change in reflected peak center wavelength  
 $\Delta d$  = change in the grating period  
 $\Delta n$  = change in the index of refraction

A more useful form of Equation 1-2 incorporates material properties of the fiber and puts them in relation to strain:

$$\frac{\Delta\lambda}{\lambda} = \beta \cdot \varepsilon \quad (1-3)$$

where:  $\Delta\lambda$  = change in reflected peak center wavelength due to axial strain  
 $\lambda$  = original peak center wavelength  
 $\beta$  = elasto-optic coefficient (changes with varying fiber types)  
 $\varepsilon$  = axial strain of the fiber

Another factor that also affects the reflected peak center wavelength is the thermal expansion and contraction of the fiber:

$$\frac{\Delta\lambda}{\lambda} = \xi \cdot \Delta T \quad (1-4)$$

where:  $\Delta\lambda$  = change in reflected peak center wavelength due to temperature change  
 $\lambda$  = original peak center wavelength  
 $\xi$  = thermo-optic coefficient (changes with varying fiber types)  
 $\Delta T$  = change in temperature

Equations 1-3 and 1-4 can then be combined to relate wavelength shifts as a function of axial strain and temperature on a fiber grating:

$$\frac{\Delta\lambda}{\lambda} = \beta \cdot \varepsilon + \xi \cdot \Delta T \quad (1-5)$$

where:  $\Delta\lambda$  = change in reflected peak wavelength due to axial strain and temperature change  
 $\lambda$  = original peak center wavelength  
 $\beta$  = elasto-optic coefficient (changes with varying fiber types)  
 $\varepsilon$  = axial strain of the fiber  
 $\xi$  = thermo-optic coefficient (changes with varying fiber types)  
 $\Delta T$  = change in temperature

Thus, these wavelength changes can be quantitatively related to strain and temperature.

The demodulation system uses an FBG as a filter to measure the wavelength of the grating under stress. Because of the relatively linear slope of the FBGs, the system has the capability to output a linear voltage with respect to fluctuations in the fiber grating sensor wavelength.

A typical fiber grating, approximately 5-6 mm (0.2-0.25 in) in length, functions as a point-source sensor. However, when packaged in a tube with additional fiber lead length and the ends attached in such a way that the grating can flex due to strain along any point between the fixed ends, essentially, the result is the creation of a long-gage sensor. The long-gage sensor can be pre-strained in manufacture so that its spectral profile is shifted by small amount (approximately 2-3 nm). This enables the measurement of both compression and tension in the sensor.



## 2.0 VEHICLE MONITORING TEST PAD

Many factors exist in determining the optimal sensitivity of a FBG traffic sensor. Each factor is important to consider in optimizing the traffic sensor for functionality, sensitivity, and range. In this process, high-priority criteria were first identified. These included housings capable of properly absorbing and collecting strain signals induced by traffic. Also significant were depth of installation, sealant (used to secure the sensor in the roadway), roadway characteristics (i.e. asphalt concrete (AC) or portland cement concrete (PCC) durability), roadway conditions (ruts, cracks, wear, etc), sensor lengths, temperature and moisture conditions. As the many needs were studied, two FBG traffic sensor designs emerged, modeled after the long-gage strain sensors used by Blue Road Research on bridges and civil structures. Two housing widths were chosen for comparison. These widths included sensors made of 1/16 in (1.6 mm) tubing with 1/4 in (6.4 mm) anchors on either end, and sensors made of approximately 1/2 in (13 mm) tubing with 3/4 in (19 mm) anchors on either end. Other factors, such as protective reinforced steel springs and steel tubing were considered, but were deemed possibly too rigid for sufficient sensor response.

### 2.1 INSTALLATION OF TEST PAD AND FBG TRAFFIC SENSORS

In the fall of 1999, two vehicle test pads were built to evaluate prototype FBG traffic sensors. The test pads were made from a 10 x 10 ft (3 x 3 m) square of PCC, at a total depth of 4 in (100 mm). This pad lies adjacent to another 10 x 10 ft square of AC, layered in two lifts for a total depth of 4 in. A drawing of the test pad is shown in Figure 2.1. By the fall of 2000, eight sensors consisting of two different FBG traffic sensor prototypes had been designed and built. Figures 2.2 and 2.3 show the housing and sensor installation.

While keeping as many constants as possible to compare the sensor types, variables were chosen in response to other critical questions such as depth and sensitivity, sealant, and PCC versus AC response. Table 2.1 summarizes the sensitivity factors considered highest priority for discovery with the test pads. Sensors were placed in parallel, approximately 24 in (0.6 m) apart, and at least 12 in (0.3 m) from the pavement edge.

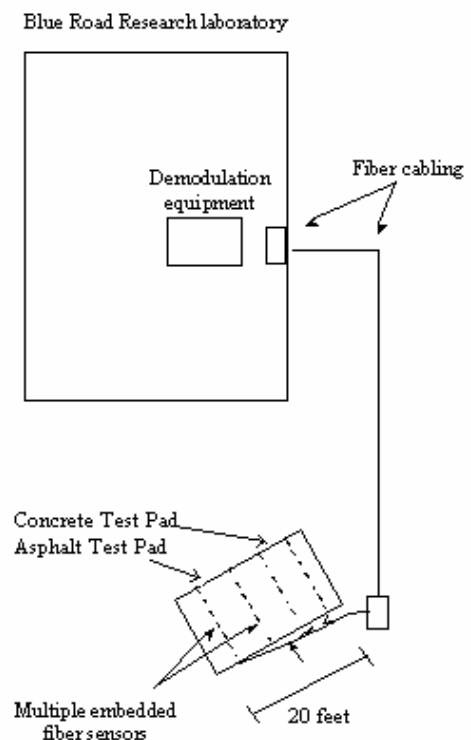


Figure 2.1: Layout of traffic test pad and sensor system



Figure 2.2: The ½" width housing chosen for FBG traffic sensor tests



Figure 2.3: A 1/16" sensor shown with the anchor

**Table 2.1: Sensor installation variables for the vehicle test pad**

Sensor No.	Sensor Pkg. Width	Sensor Length	Road Material	Slot Depth	Sealant
1	1/16"	59"	AC	2"	Epoxy
2	½"	79"	AC	2"	Epoxy
3	1/16"	59"	AC	3"	Hot bituminous sealant
4	½"	79"	AC	3"	Hot bituminous sealant
5	1/16"	59"	PCC	1"	Epoxy
6	½"	79"	PCC	1"	Epoxy
7	1/16"	59"	PCC	2"	Hot bituminous sealant
8	½"	79"	PCC	2"	Hot bituminous sealant
temp.	½"	79"	PCC	2"	Hot bituminous sealant

The procedure developed for installation was similar to that of loop inductors. First, a channel was cut into the roadway. The active sensing area (the portion between each anchor) was placed near the bottom of the slot. The slot was filled with a sealant that had moisture insensitive, flexible, and low exothermic properties. An epoxy and bituminous sealant from the ODOT approved products list was used. After the sealant cured, the sensor lead was connected and ready for monitoring.

All nine of the sensors placed into the test pads were successfully installed and responding. Figure 2.4 to 2.8 show various segments of the sensor installation into the test pad.



Figure 2.4: Cutting slots for the FBG traffic sensor installation



Figure 2.5: Optimizing sensor channels for ideal fit prior to installation. Heater boxes (right) were used for curing



Figure 2.6: Placing the 1/2" sensors into the AC test pad



Figure 2.7: Hot bituminous sealant was used to fill the channels for half of the sensors. The protruding mound was later removed so the surface can be completely level



Figure 2.8: AC test pad (left) and PCC test pad (right) after the traffic sensors were installed and sealants dried

## 2.2 DATA OBTAINED FROM THE TEST PAD

Data obtained from the use of vehicles on the test pads gave engineers a basis for determining sensitivity levels of the sensors and their response under varying installation conditions. The primary vehicle used in data collection and measurement was a 3,200 lb (1,450 Kg) 4-door sedan. Figure 2.9 shows a typical response obtained from one of the sensors as the right wheel of a vehicle backs across the sensor placed at a 2 in (50 mm) depth in the AC.

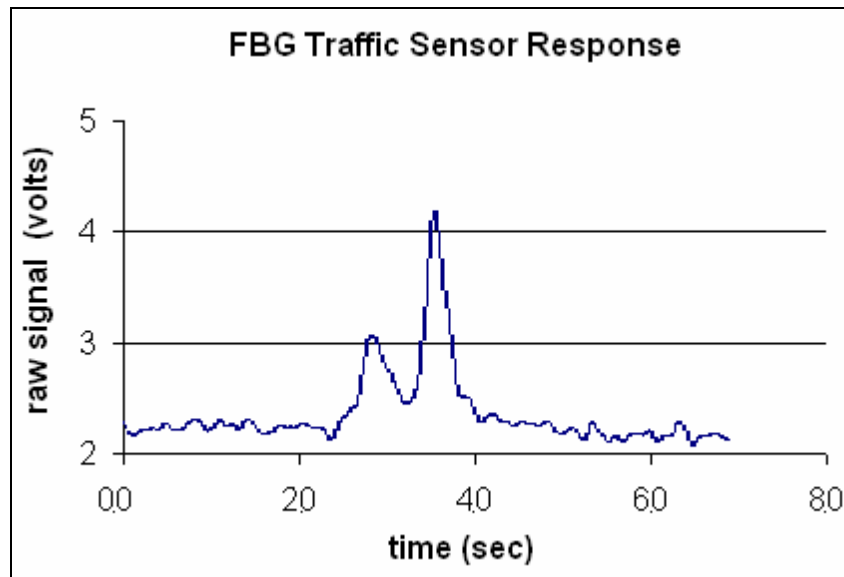


Figure 2.9: Sensor response to a vehicle backing across the sensor

### 2.2.1 AC Response on the Test Pad

On the AC portion of the test pad, variation in the response of the signal at speeds from static to 10 mph (16 km/h), due to the distinct widths of the sensor, did not affect the gain of the signal by

greater than 10%. However, signal amplitudes dropped as a function of installation depth, suggesting that larger responses may be achieved by installation closer to the surface. Responses to the various sealants also appeared to be fairly uniform, with the hot bituminous sealant being only slightly more responsive during testing.

A person was detected walking and jumping directly on each sensor line of the AC test pad. At a 2 in (50 mm) depth, a person is easily detected standing with one foot on either side of the sensor line.

### **2.2.2 PCC Response on the Test Pad**

The PCC responses paralleled those of the AC test pad, but were approximately 25% less sensitive in amplitude response. Sensitivity of the 3 in (76 mm) deep sensors was difficult to measure in non-ideal conditions, shifting spectrally not more than 1 to 2 picometers. One of the ½ in (13 mm) sensors floated to the surface during epoxy cure. Although it protrudes from the surface by approximately 3/8 in (10 mm), it responded in similar ways as the other sensors, but was slightly more sensitive. This increase in sensitivity was likely due to the direct transfer of strain from the vehicle to the sensor.

## **2.3 CONCLUSIONS FROM TEST PAD STUDY**

In general, the test pad exercise served to prove the feasibility of operations for FBG traffic sensors. It demonstrated that the pavement (AC or PCC) transfers strain from the weight of a moving vehicle into the packaged sensor proportionally to the vehicle size and distance from the sensor.



### 3.0 TESTING PROTOTYPE FBG TRAFFIC SENSORS

Results obtained from the test pad were helpful in understanding the relationships between depth, sensitivity and stiffness of AC versus PCC. But a high volume highway installation was needed to address performance on speed variations, long-term sensor durability, and high-usage conditions.

#### 3.1 INSTALLATION OF THE FBG TRAFFIC SENSOR IN THE INTERSTATE 84 FREEWAY WESTBOUND LANE

In August of 2001, four FBG traffic sensors and one temperature sensor were installed into the westbound right lane of the Interstate 84 freeway (I-84), near Exit 14 (Fairview). The average daily traffic across 6 lanes was 57,900. Figure 3.1 diagrams how the 1,120 ft (341 m) fiber cable line with 12 available channels was routed from the freeway junction box to the Blue Road Research facility where the demodulation equipment is housed.

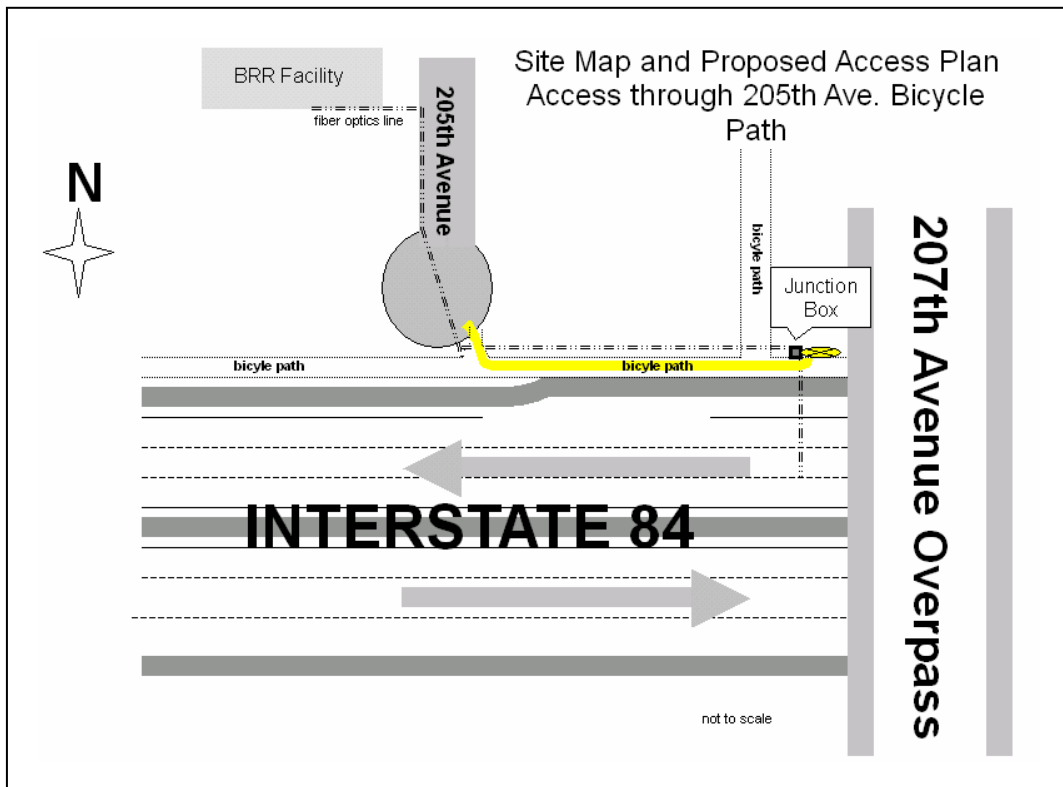


Figure 3.1: Site map of the final layout for FBG sensors

Figure 3.2 shows the installation layout in the westbound lane. The on-ramp and right lane of the freeway were closed for a short time while the sensors and cabling were placed. Some of the steps in the sensor installation can be seen in Figures 3.3 to 3.8.

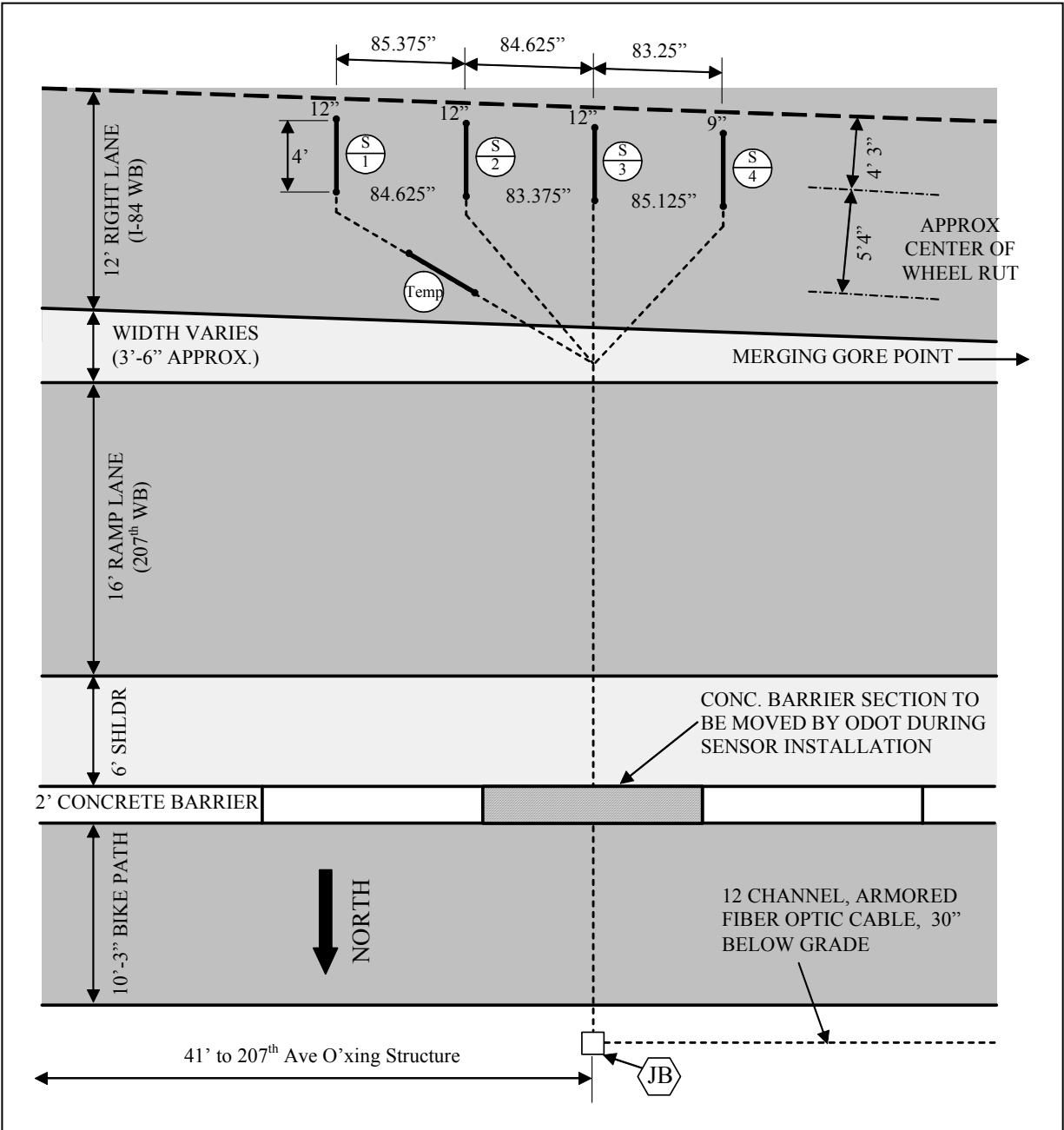


Figure 3.2: Layout of FBG traffic sensors on the westbound lane of I-84 freeway



Figure 3.3: Saw cuts were made into the freeway in a fan-out pattern



Figure 3.4: Trench for the fiber backbone carrying the traffic signals to a remote readout facility

Saw cuts were made in the PCC at a depth of  $2\frac{3}{4}$  in (70 mm). The 48 in (1.2 m) long sensors were placed into the westbound right lane, across the left wheel path of the traffic lane. Table 3.1 details the sensor and anchor diameters. Hot bituminous sealant was used to secure the sensors into the roadway and fill in the sawed channels. The sealant was leveled evenly with the road surface so the sensor would measure primarily the strain from the pavement rather than the sealant. The level surface was also important to minimize changes in response or calibration as the sealant wore away.

**Table 3.1: FBG sensor layout**

Sensor No	Sensor Package Diameter	Anchor Diameter	Slot Depth
1	1/16"	1/4"	2 $\frac{3}{4}$ "
2	1/2"	3/4"	2 $\frac{3}{4}$ "
3	1/16"	1/4"	2 $\frac{3}{4}$ "
4	1/2"	3/4"	2 $\frac{3}{4}$ "
Temperature	1/16"	1/4"	2 $\frac{3}{4}$ "



Figure 3.5: Marking was placed for the saw cut



Figure 3.6: Sensors were placed into the freeway

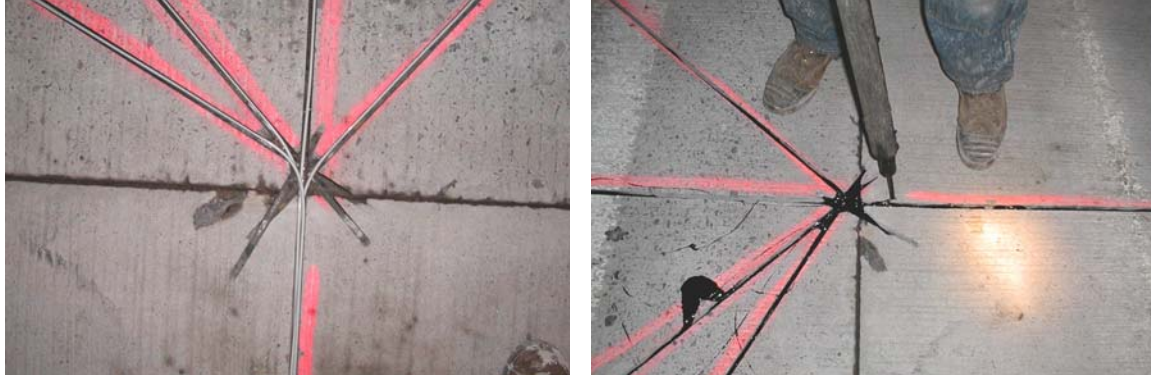


Figure 3.7: The sensors can be seen as they were routed through the junction point and then fan out to their respective locations in the AC (left). The junction point and sawed channels were later filled with hot bituminous sealant (right).



Figure 3.8: The ground-level junction box (left) as it was prepared for protecting the connections between the freeway sensors and the fiber line. Right, an overview of the sensor area and the junction box.

## 3.2 DATA OBTAINED FROM THE I-84 FREEWAY

Data acquired from traffic on the freeway was collected via computer using customized LabVIEW acquisition software. This allowed sampling of the FBG traffic sensors (as an analog voltage) at various sampling rates, because collecting continuous analog signals would generate large volumes of data and require extensive computer memory storage.

### 3.2.1 Evaluation of the Sensors Placed in the I-84 Freeway

About two weeks after the installation, the four traffic sensors and the temperature sensor were tested using the high-speed demodulation (HSD) system. No response or spectral peak was found from Sensors 3 or 4 and the other two sensors exhibited unusual responses. An optical spectrum analyzer revealed the spectral peak in Sensors 1 and 2 decreased about 3 nm from its pre-installed setting (see Table 3.2). The temperature sensor was functioning as expected.

An attempt was made to locate damage in the fiber using an optical time domain reflectometer, but no useful information was obtained due to the instrument’s resolution. Detection couldn’t be resolved any closer than 6 to 10 ft (2 to 3 m) from the sensor. Table 3.2 shows the spectral peak for each sensor during different phases of construction.

**Table 3.2: Chart showing spectral values (in nm) for the traffic sensors**

Sensor	Original unstrained value ( $\lambda_0$ )	Pre-strained value ( $\lambda_p$ )	Post-installed value ( $\lambda_1$ )
1	1297	1299	1297.5
2	1300	1303	1300
3	1297	1299	-
4	1297	1300	-
Temperature	1300	1300	1300

Although it was common to see changes of less than 1 nm from  $\lambda_p$  to  $\lambda_1$  (due mostly to strain inadvertently placed on the sensor during installation), it was not common to see these values return to their original wavelength,  $\lambda_0$ . This evidence strongly suggests that the pre-strain was lost. After careful study, it was concluded that all four traffic sensors had been damaged. It appears Sensors 3 and 4 were detached from their housings on the near side of the grating, thereby yielding no spectral reflection. Sensors 1 and 2 were detached on the far side of the grating, yielding a spectral reflection, but at a loss of the pre-strained values. The temperature of the hot bituminous sealant was investigated as a possible cause of sensor damage, but there was no conclusive evidence that this was a factor.

In addition, data collected on the temperature sensor (intentionally detached on the far side of the grating to prevent pre-strain by design) yielded traffic responses similar to Sensors 1 and 2, although not as uniformly. The lack of uniformity is probably due to the diagonal position of the temperature sensor relative to the other sensors and the roadway.

Without pre-strain on the traffic sensors, it was surprising to learn that small and large vehicle sizes were still detectable, some of them with very well-defined profiles. Relative signal amplitude differences still existed among vehicles of various sizes. However, strain responses were several times larger than those seen on the test pad, even while one end of the grating was detached in the housings. Possible causes of this may be due to a greater installation depth or higher traffic speeds, which change the strain fields inside the concrete.

### 3.2.2 Sensor Response and Durability

After six months of testing, the sensors had not experienced any further deterioration in performance or sensitivity. Since sensor durability is proportional to strain on the grating, and the grating is essentially loose within the housing, it is theoretically possible that the FBG traffic sensors may last for the life of the roadway. Figure 3.9 shows raw data collected for a semi-tractor trailer on Sensors 1 and 2.

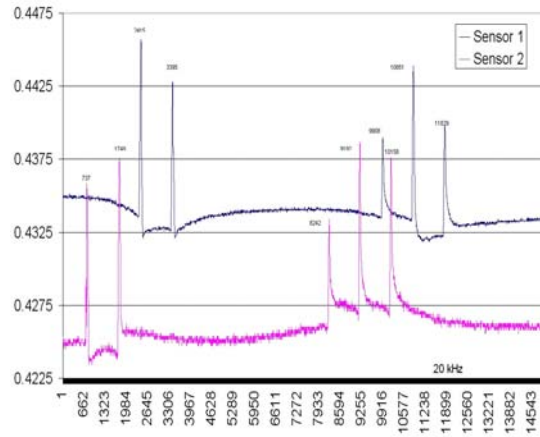


Figure 3.9: Left, semi-tractor trailer crossing embedded FBG sensors, traveling left to right. Response from two FBG sensors (right). From this data, velocity (57 mph), axle spacing and potentially weight may be determined.

Other data captures can be seen in Figures 3.10 and 3.11. The velocity of the vehicle was determined by dividing the sensor spacing by the time it took to travel from Sensor 1 to Sensor 2. The axle spacing was determined by dividing the previously calculated velocity by the time for subsequent axles to cross the same sensor. Velocity and axle spacing were calculated using the data shown in Figure 3.10:

$$\text{Velocity} = \Delta\text{Distance} / \Delta\text{Time}_{1-2} = (7 \text{ ft}) / (0.491 \text{ sec} - 0.404 \text{ sec}) = 80.5 \text{ ft/sec} = 55\text{mph}$$

$$\text{Axle Spacing} = \text{Velocity} * \Delta\text{Time}_{1-1} = (80.5 \text{ ft/sec}) * (0.404 \text{ sec} - 0.370 \text{ sec}) = 2.74 \text{ ft}$$

The temperature sensor was installed to monitor variations in pavement temperature for future sensor calibration needs. Data indicates that the temperature can be resolved to better than 1°C (34 F). With better compensation for strain (noise) or further noise-reduction in the electronics, this likely can be improved to within one or two-tenths of a degree accuracy.

The ideal traffic sensor should be sensitive to vehicles ranging from semi-tractor trailers to bicycles. Because the FBG sensor measures strain, it responded easily to large vehicles such as trucks and buses (see Figure 3.9). The smallest vehicles seen crossing the sensors included small cars such as the Chevrolet Chevette and Subaru Justy (see Figure 3.12).

Although modifications were made to the sensor housing design to improve system repeatability and boost small-vehicle sensitivity, data collected from the freeway accurately represented the vehicle speeds. High traffic volumes and remote distances to the monitoring equipment made it difficult to correlate the vehicles with corresponding signals. However, only data that was visually verified was used for analysis. In each of these, signal amplitude appears to be closely proportional to vehicle weight, strongly suggesting that WIM capabilities exist within the FBG traffic sensor, as noted by other research (*Lai 1997, Terai 1998*).

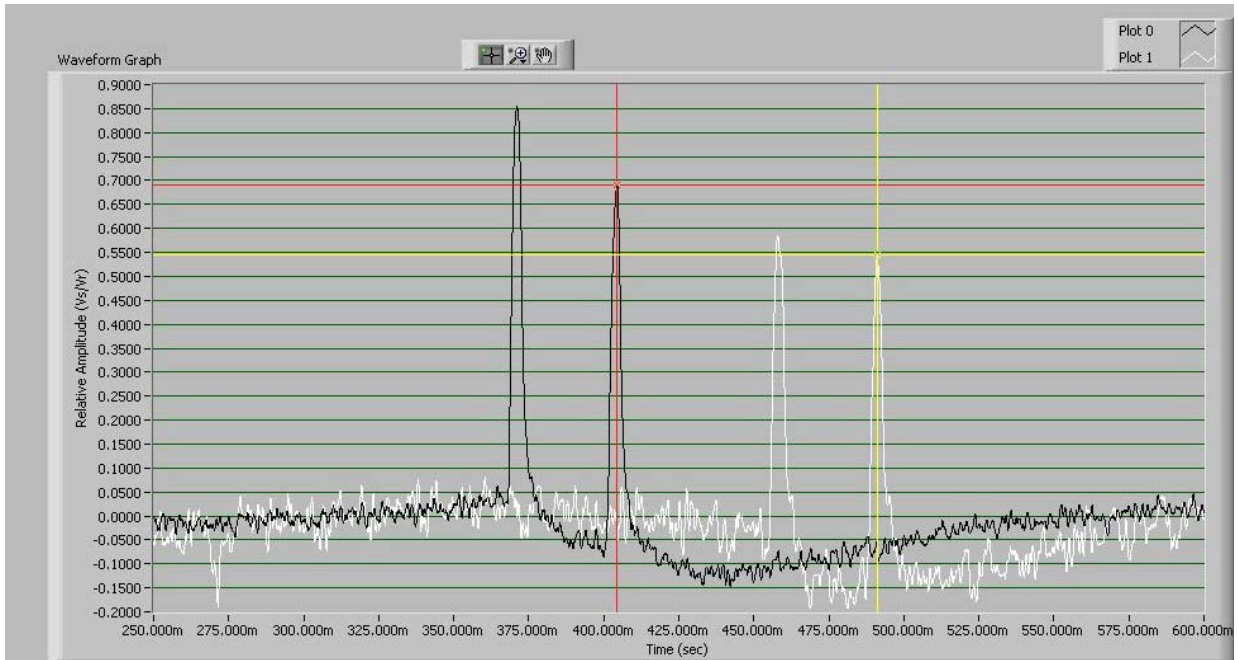


Figure 3.10: Data capture from a vehicle traveling 55 mph with 2.74 ft axle spacing

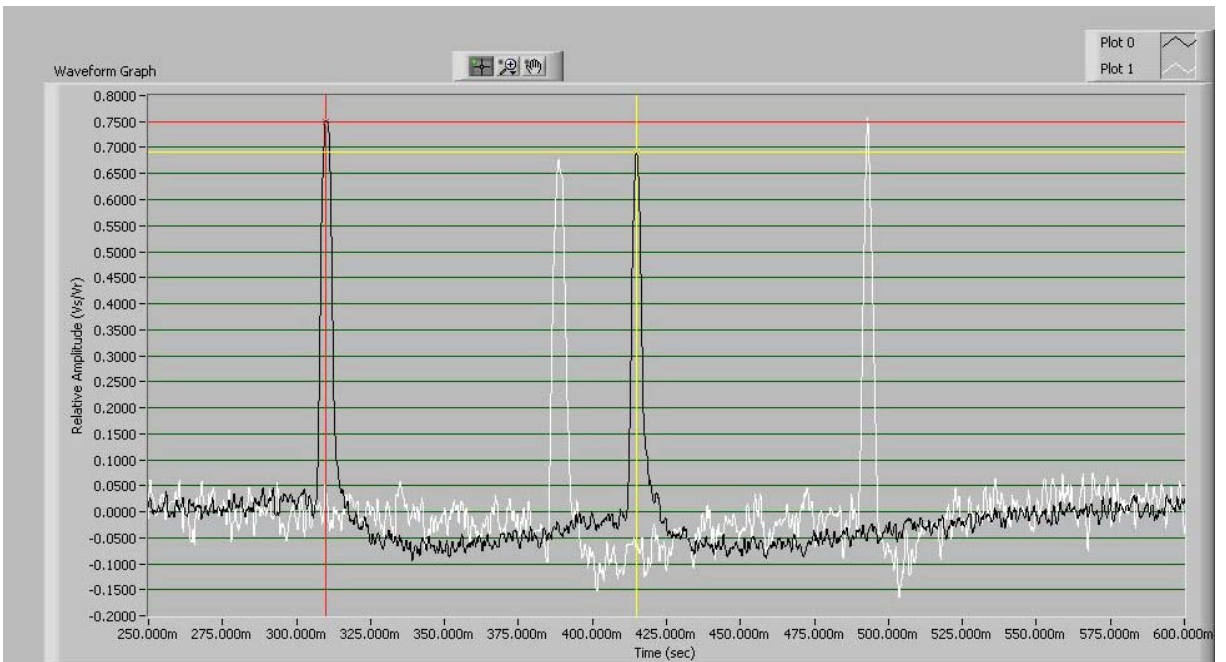


Figure 3.11: Profile of a small vehicle traveling 61 mph with 9.5 ft axle spacing

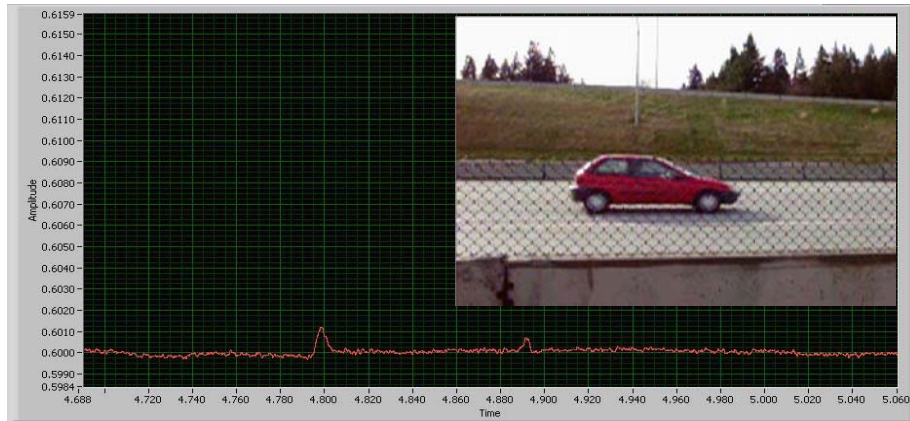


Figure 3.12: A Geo Metro and its profile are shown above. The graph shows relative amplitude versus time in seconds

### 3.3 RESULTS OF INTERSTATE 84 MONITORING

As seen in Figures 3.9 to 3.12, the FBG traffic sensors may detect a range of vehicle classes. Their acquisition rates may be useful for collecting WIM information. For standard traffic classification, compatibility and integration to conventional traffic classifiers, the FBG sensor functions well.

Figure 3.13 shows several vehicles detected in the adjacent lane. The traffic response appears as rolling peaks rather than spikes on the chart.

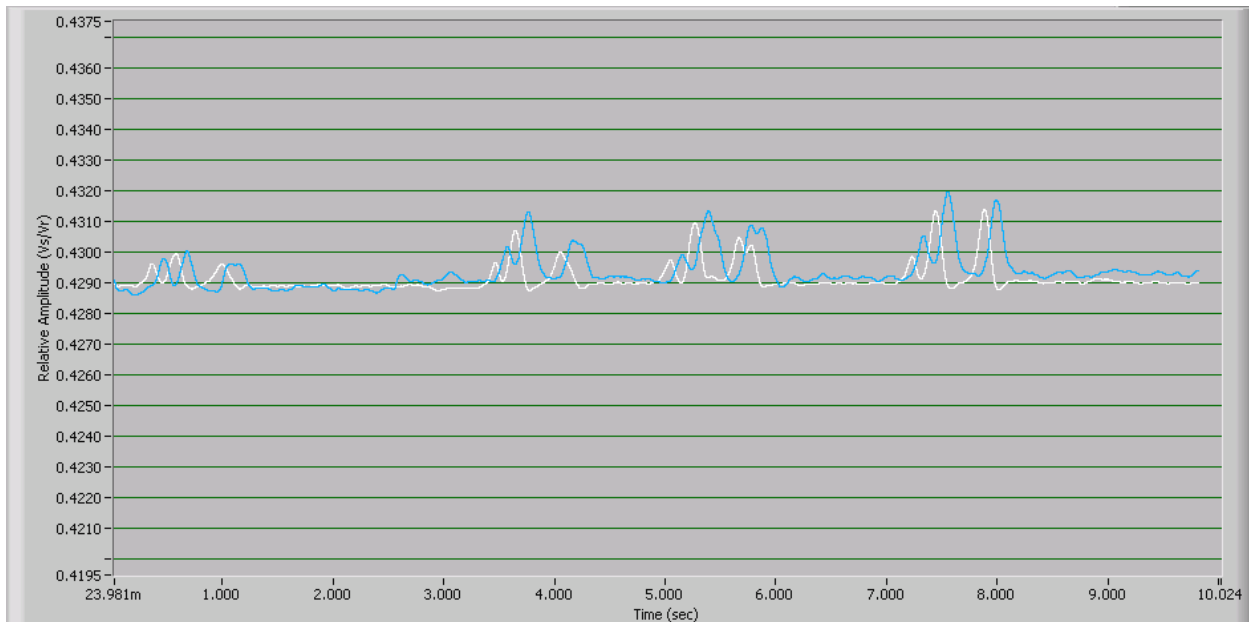


Figure 3.13: A series of vehicles detected in the adjacent lane

This information is interesting in that it may be possible to detect traffic in the adjacent lane as a separable and distinct signal. This could be accomplished by installing additional sensors transverse to each other and optimizing the demodulator system. Potential uses of this information may include monitoring of multiple lanes from a single location, or enabling vehicle detection from the road shoulder.



## 4.0 REDESIGNING THE FBG TRAFFIC SENSORS

Although the original sensors did detect passing vehicles, their ability to detect all traffic was uncertain. A more reliable sensor was needed to assure a consistent response.

### 4.1 CONSIDERATION FOR A REDESIGNED SENSOR

In May 2002, ideas to enhance performance of the sensors were pursued, focusing primarily on the sensor housing. The key elements for redesign were as follows:

- **Sensitivity:** If the fiber optics truly became detached inside the housings, as the evidence suggested, and the systems were still able to monitor and distinguish vehicle classes by signature, then keeping the gratings under pre-strain ( $\lambda_p$ ) should contribute to a significantly higher sensitivity and resolution.
- **Durability/Longevity:** If sensor depth can sufficiently shield it from vehicle tire exposure, it should last until repaving or reconstruction is necessary.
- **Ease of Installation:** The installation of the fiber optic traffic sensors was fairly straightforward. The procedure was similar to that of a conventional traffic sensor loop installation, except that a straight line was cut into the pavement instead of a circle. It should be noted that the fiber cabling requires careful layout planning to assure that lead lengths are sufficient; and bending radius should be limited to 3 in (76 mm) or more.
- **Repeatability:** This issue was believed to be the most critical point to address. Because the sensors appeared to be detached on one end, vehicles of the same physical characteristics could have varying effects on the sensors' response, due to random variation in the location of the grating inside the packaged traffic sensor. The data suggested this as well, as sometimes the axle spikes were upward, and sometimes downward. A possible reason for this may be the axial strain in the grating changing from compression to tension on the grating as traffic passed over.

An analysis of the four sensor responses pointed to the most likely problem being the detachment of the gratings inside the housing, on either the far, or near side of the 5 to 6 mm (0.2 to 0.25 in) grating. Evidence suggested Sensors 3 and 4 completely lost their reflected signals by a physical break in the sensor line. All four sensors lost their pre-tension settings, also indicative of a break in the sensor line. Looking at the remaining two signals, neither signal had a widening in its Full-Width, Half-Max (FWHM), indicating that the entire grating was intact. The 1 to 2 in (25 to 50 mm) area immediately near the grating is considered the most susceptible to damage, due to the Bragg grating creation process, where the optical coatings are removed to laser-engrave the

grating, and then the fiber is recoated. The next most likely places for a physical break are at the endpoints or in the splice area. Figure 4.1 shows the possible areas of damage to the sensor housing.

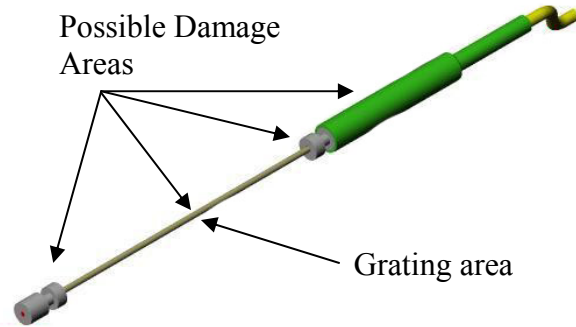


Figure 4.1: Possible physically-damaged areas in sensor housing

Although not proven, sensor overstrain from traffic is the leading theory for failure of the original prototype design. Therefore, providing sufficient protection against overstrain became a high criteria.

## 4.2 REVIEW OF PROPOSED DESIGNS

Four new designs were considered for the second field test.

Design 1: A composite-reinforced sensor that would protect the sensor by limiting the strain force on the sensor is shown in Figure 4.2. The advantages of enclosing the original system inside a composite encasement was the protection it provided to the tubing and grating by absorbing extremely high strain forces.

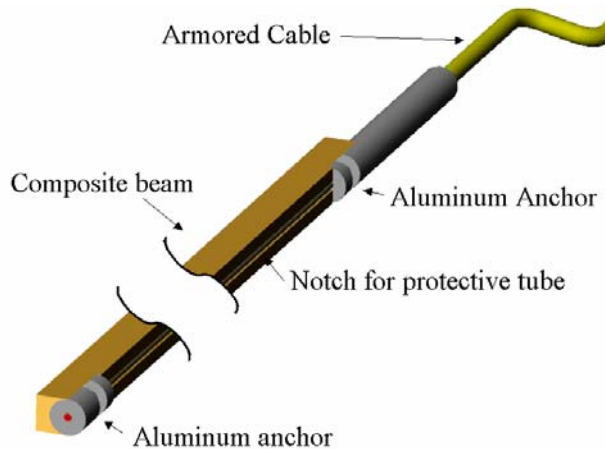


Figure 4.2: A composite beam encloses a long-gage traffic sensor

- Design 2: A spring-actuated sensor could be used to dampen the strain-effect of traffic. The advantage of something similar to Figure 4.3 is that the spring would allow for tension to be released if extremely large strain forces become present.

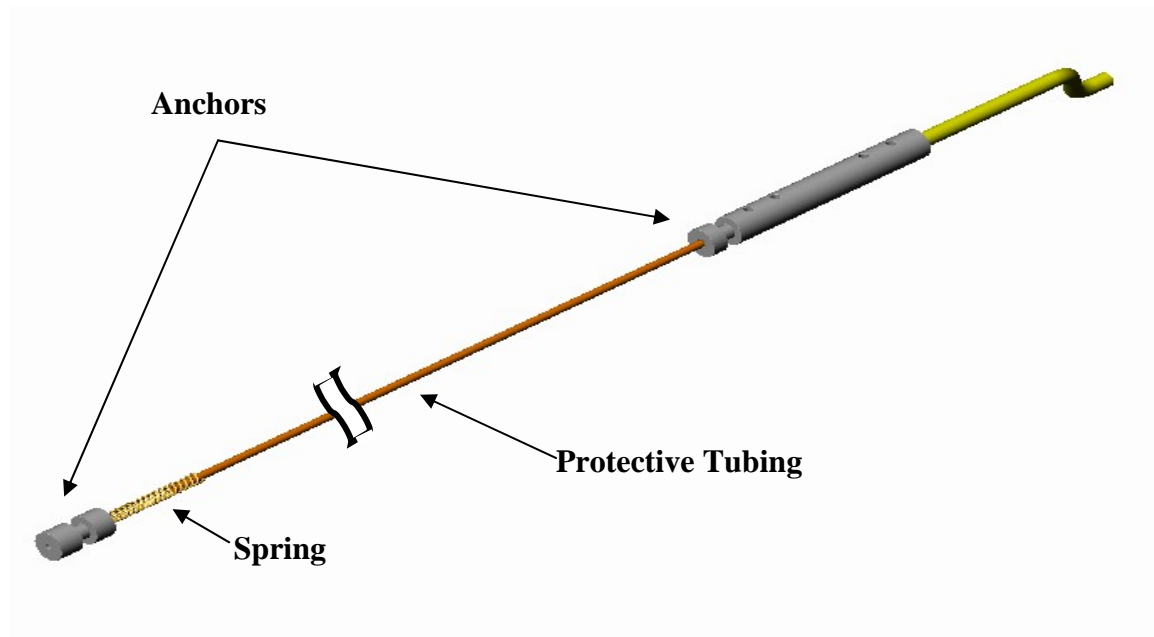


Figure 4.3: Possible sensor redesign using a spring to dampen strain

- Design 3: Enhancements could be made to the first-generation traffic sensors since the initial installation, including additional splice protection (reinforced steel pin) and a crimped anchor support, and enhancing the housing strength by several times.
- Design 4: Direct embedment of the fiber grating area in a composite beam without a protective tube is shown in Figure 4.4. An unsleeved fiber grating would allow the strain from traffic to be directly transferred to the grating area without length integration as the composite beam flexes due to traffic. It would provide a simplified manufacturing method, reducing cost and manufacture time.
- Other ideas investigated included the use of full lane-width sensors, additional ideas based on non-overstrain cases, and variations to the installation procedure.

The designs chosen for the second field test included the long-gage composite-reinforced sensor (LGC - Design 1) and a long-gage enhanced sensor (LGE - Design 3). In addition, the unsleeved composite sensor (UNC - Design 4) was chosen because it was believed to be the most survivable, but was lacking a uniform response across the wheel path.

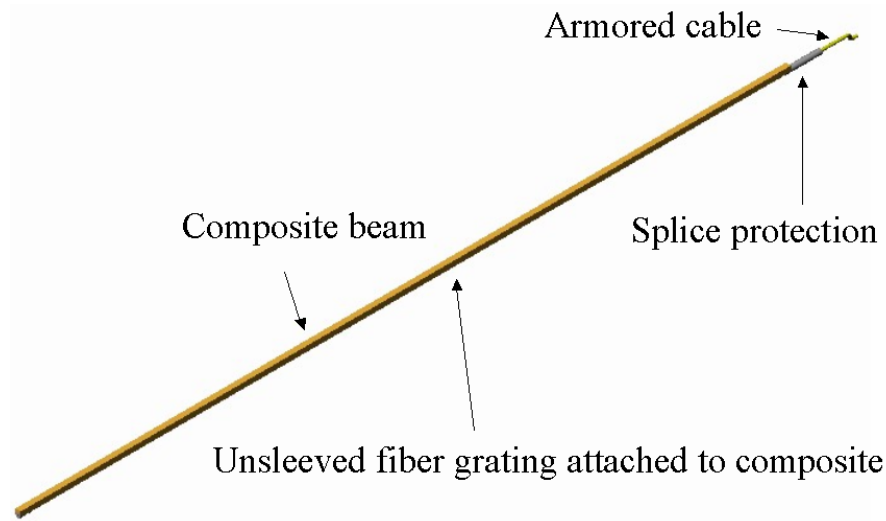


Figure 4.4: Design for composite reinforcement of optical traffic sensors

### 4.3 FREEWAY LAYOUT AND MANUFACTURING

The layout for the second-generation sensors is shown in Figure 4.5. They were installed August 20, 2002 on I-84, adjacent to the original sensors.

#### 4.3.1 Manufacture & Installation of FBG Traffic Sensors

Sensors 5 and 7 were attached to  $\frac{1}{4}$  in x 4 ft (6.4 mm x 1.2 m) composite beams. Sensor 8 was attached to a  $\frac{1}{4}$  in x 2 ft (6.4 mm x 0.6 m) beam. The epoxy used in the manufacturing process was allowed to cure for one week prior to installation. Table 4.1 provides details about the sensors, and Figures 4.6 to 4.9 show the sensors before and during the installation.

**Table 4.1: The configuration of the second-generation fiber optic traffic sensors**

Sensor	Width (in)	Height (in)	Length (in)	Configuration
5	$\frac{1}{4}$ "	$\frac{1}{4}$ "	48"	long-gage composite (LGC)
6	$\frac{1}{16}$ "	$\frac{1}{16}$ "	48"	long-gage enhanced (LGE)
7	$\frac{1}{4}$ "	$\frac{1}{4}$ "	48"	long-gage composite (LGC)
8	$\frac{1}{4}$ "	$\frac{1}{4}$ "	24"	unsleeved composite (UNC)

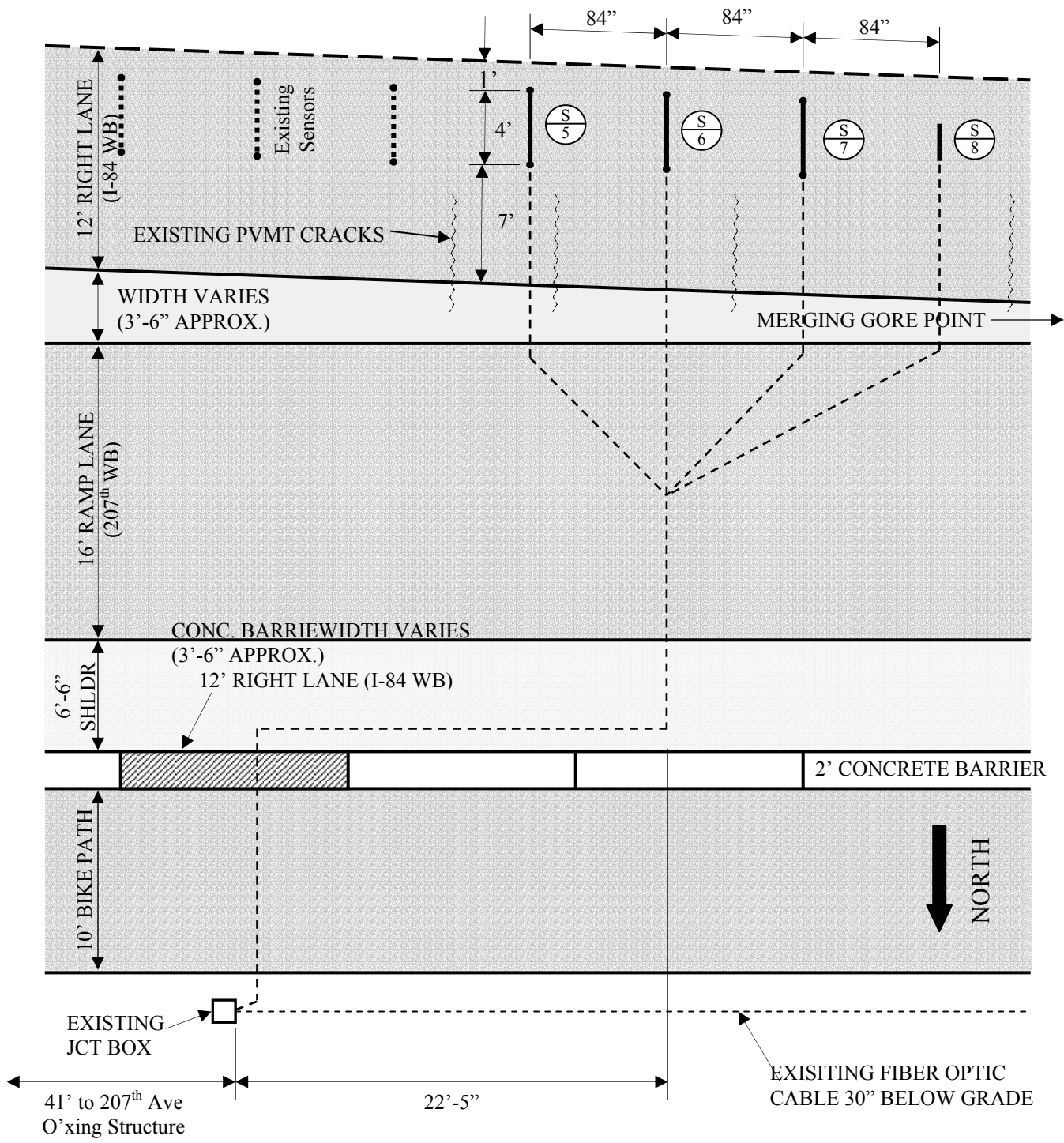


Figure 4.5: Sensor layout and placement for second installation

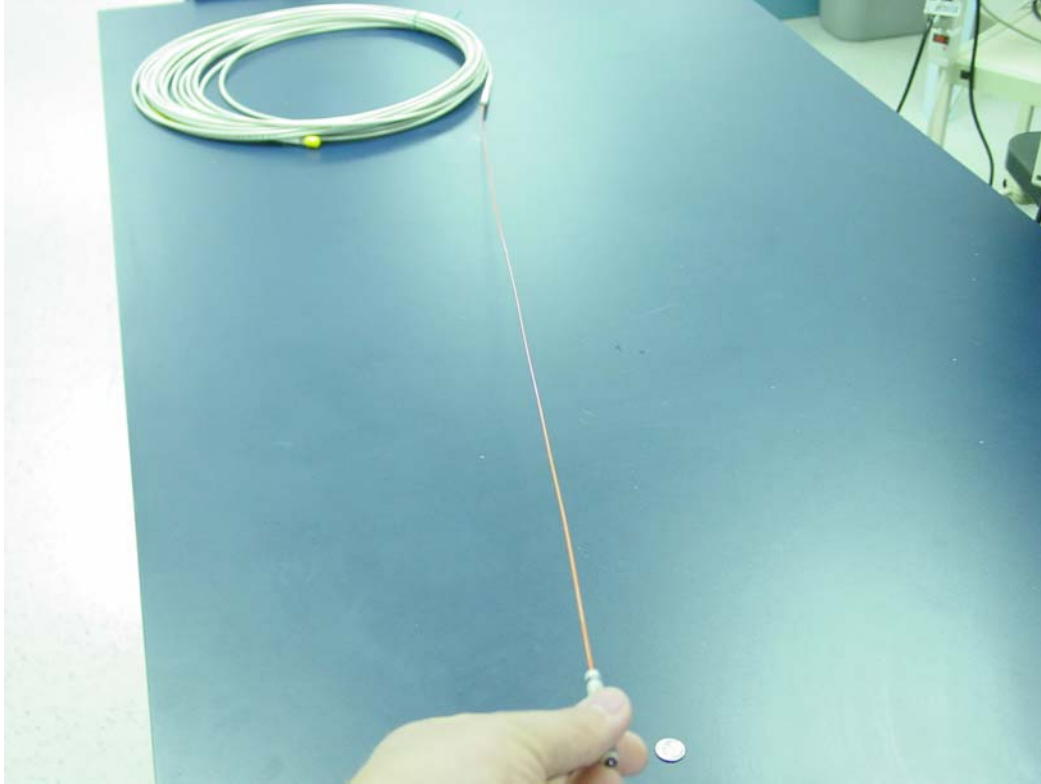


Figure 4.6: Enhanced FBG traffic sensors used in the I-84 freeway (Sensor 6)

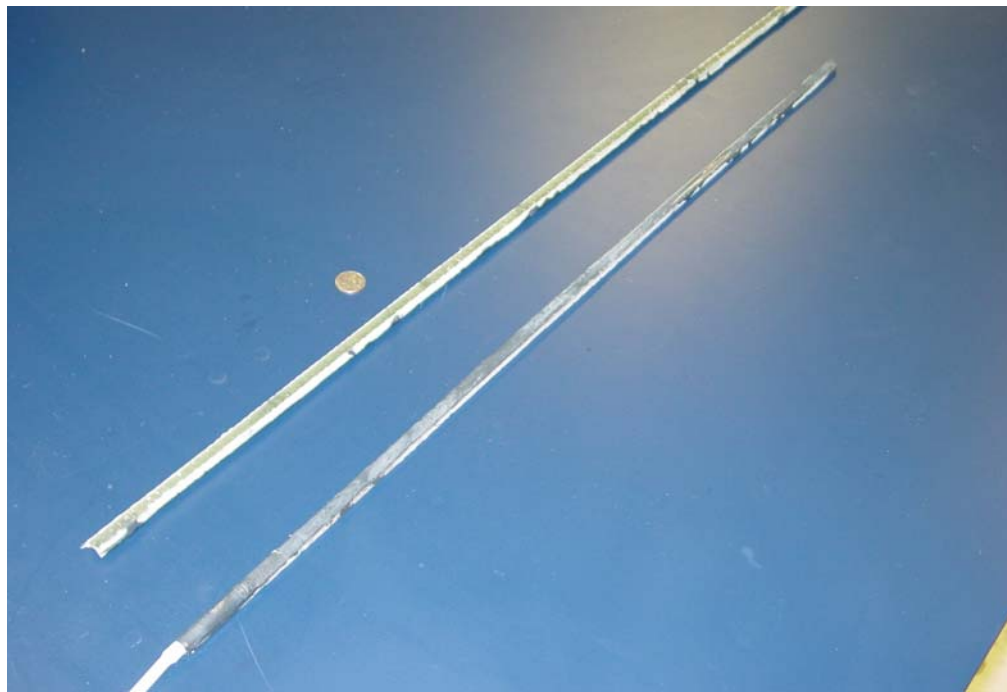


Figure 4.7: Long-gage composite FBG traffic sensors (LGC) configuration.  
The composite beam provides rigid support to prevent overstrain

Installation of the sensors occurred without incident. Each individual sensor was monitored during the installation using the backbone line and equipment from the original installation. Saw cut depth was 3 in (76 mm), slightly deeper than the original installation. Unlike the first installation, ½-in (13 mm) diameter foam pieces (shown at the bottom of Figure 4.8) were placed below and above each sensor line to allow sealant to flow below the sensor beam. The sealant was applied in layers to prevent excessive heat build up, following standard practice.



Figure 4.8: A composite sensor after being placed in the saw cut, awaiting bituminous sealant to complete the installation



Figure 4.9: The sensor after one pass of bituminous sealant is applied

## 4.4 EVALUATION OF REDESIGNED FIBER OPTIC SENSORS

All four of the sensors installed in August 2002 remained fully functional with no indication of changes to the original pre-strained set during manufacture. Each separate sensor design appeared to yield varying responses to traffic, based on its type or design, but all sensors produced peaks corresponding to wheel passes. Figure 4.10 shows a profile of the second-generation sensors (Sensors 5-8) about 10 minutes after sealant was placed, as a 190 lb (86 kg) person bounced a few times near each sensor.

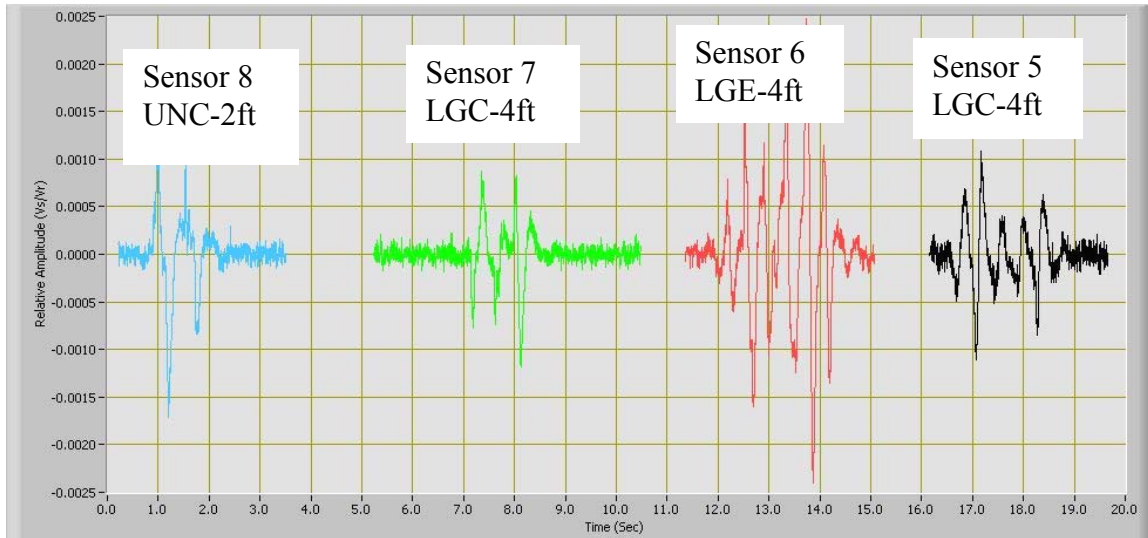


Figure 4.10: Responsiveness is tested by jumping a few times near each sensor

Each of the three sensor types (LGC, LGE and UNC) had distinctly different responses. An interesting effect was the reaction of the enhanced long-gage (LGE) traffic sensor with its counterpart, the long-gage traffic sensor embedded in the composite (LGC). Figure 4.11 and 4.12 show the effect of each sensor as traffic crosses. In these figures, the first peak shown (dotted line) is that of the LGE. Although the reaction to the 5-axle vehicle was nearly identical, the LGE sensor tended to drop to the baseline slightly faster than its composite counterpart at a 10 KHz scan. Figure 4.12 also shows this effect, noting the differences in baseline between the axles 2-3 and 4-5. The solid line shows the peak of two axles, but blends them into one axle.

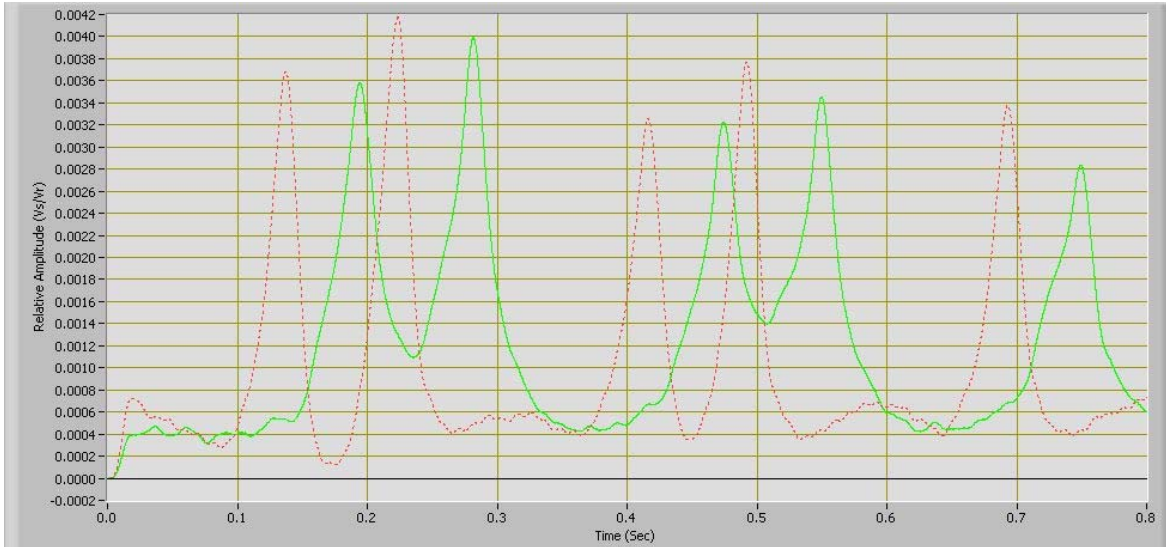


Figure 4.11: The LGE (first peak/dotted line) and LGC sensors, respectively, react to a 5-axle vehicle

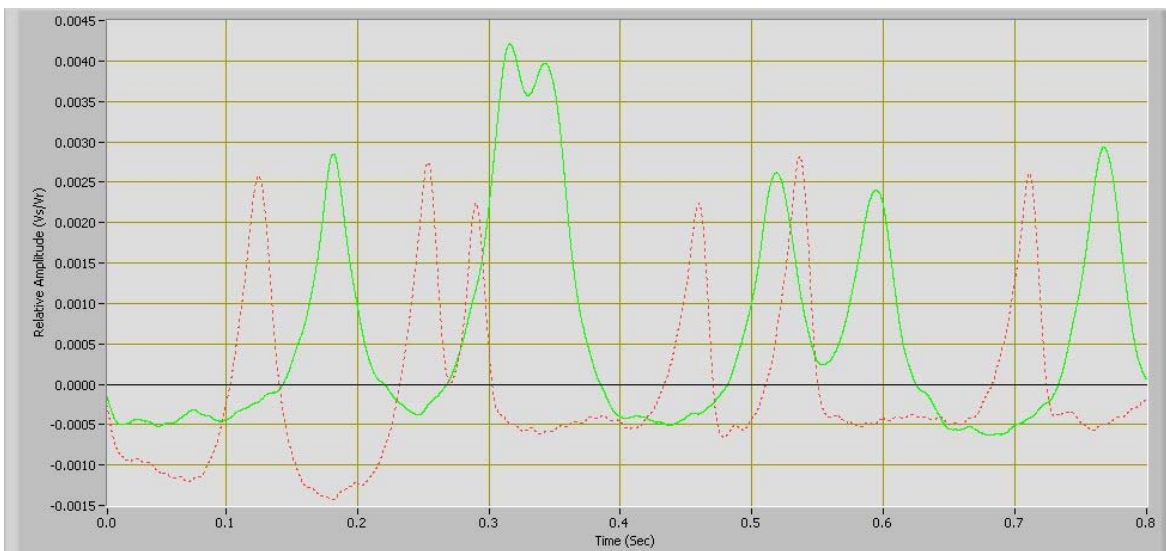


Figure 4.12: The LGE sensor (first peak/dotted line) appears to recover slightly faster than the LGC sensor

Figures 4.13 and 4.14 show the reaction of the UNC compared to its counterpart, the LGC (dotted lines).

Overall, the UNC sensor appeared to be very sensitive to strain. This was expected because the grating area is not integrated over a larger distance. A strain in the direct vicinity of the grating, or 6 in (150 mm) on either side, produces the best response, but response decreases as the load-to-grating distance increases.

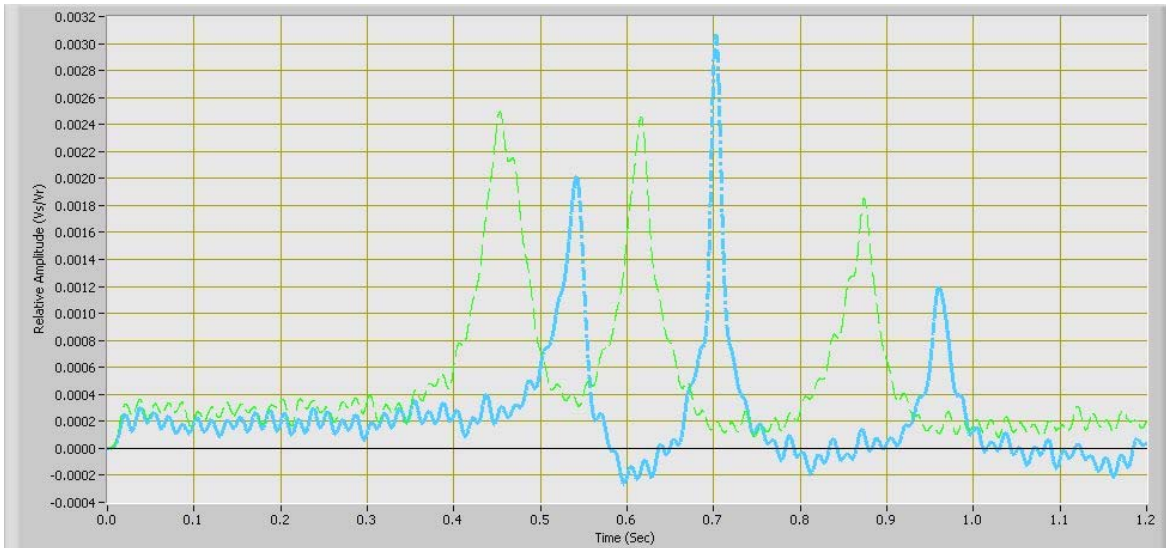


Figure 4.13: The LGC (lighter dashed line) and the UNC sensor react to traffic passing over

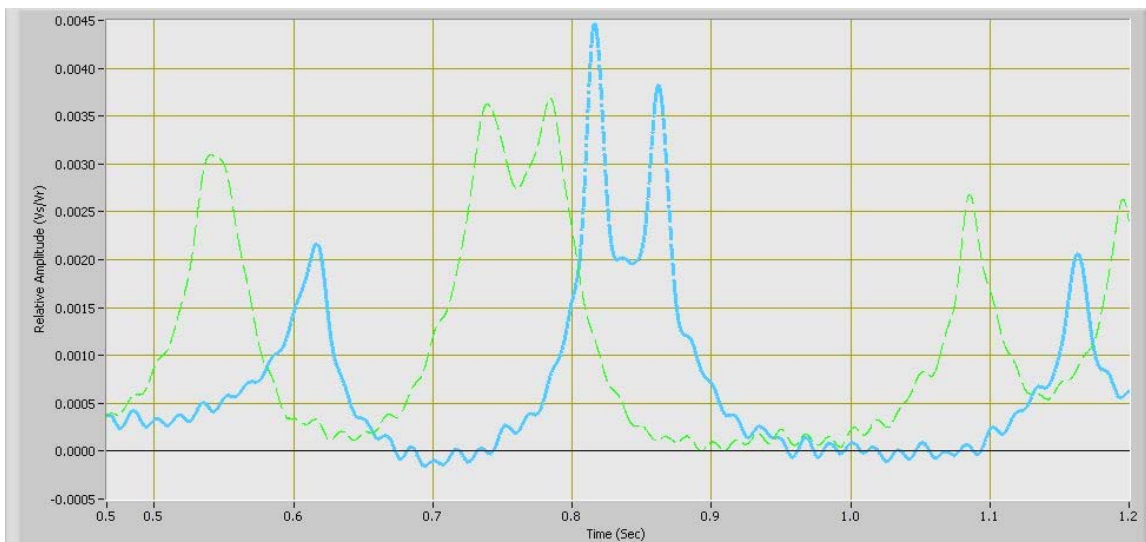


Figure 4.14: The LGC (lighter dashed line) and the UNC sensor react to traffic.  
The UNC appears to recover slightly faster

The UNC sensor appeared to recover faster to passing traffic, but the amplitude is based on the position of the wheel at crossing, thus the higher or lower amplitudes which are seen in Figures 4.13 and 4.14. Note that no distinction has been made as to whether the amplitude dependence is due to the difference in beam length (2 ft versus 4 ft) (0.6 m versus 1.2 m), or the difference in the design configuration and manufacture (UNC versus LGC).

There are still some unresolved issues as to the performance of the sensors, although repeatability seemed to have improved with the second-generation sensors. There was some time-dependent drift based on the road heating and cooling, but this is very slow and can be

corrected by temperature compensation. One of the inherent problems of the detached, original-installation sensors was that the baseline drifted up or down after vehicles were detected. The baseline of three of the second-generation sensors appeared stable, but Sensor 5, LGC, had a noticeable shift in the baseline, as shown in Figure 4.15. Sensor 5 is shown as the darker line. From the data collected, Sensor 5 had the most noticeable shift.

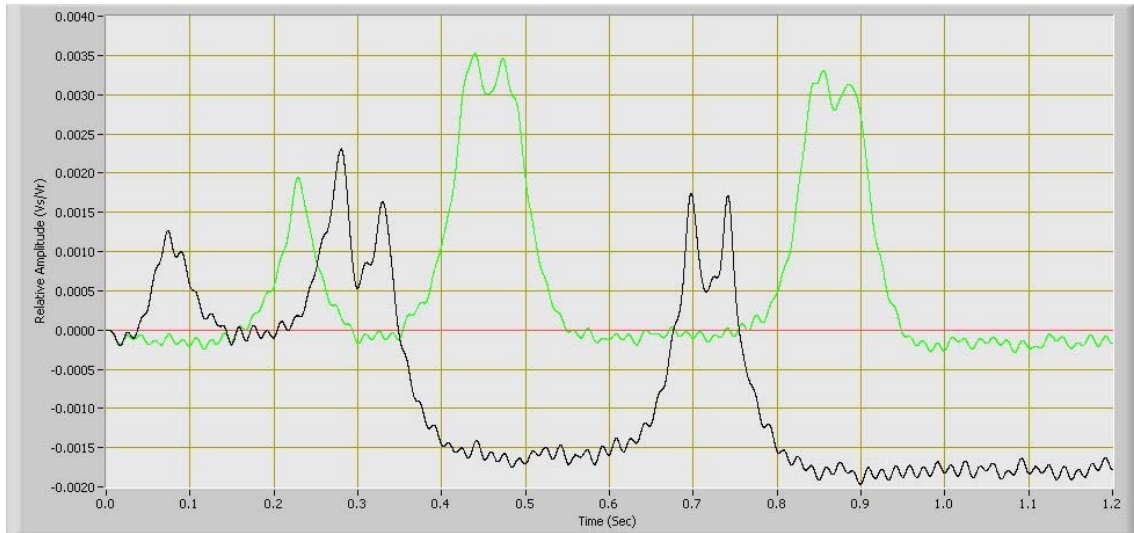


Figure 4.15: Two identical LGC sensors profile a vehicle. A baseline offset occurs in one line.

Noise may also be a contributing factor to the inherent quality of the sensor readings as seen in Figures 4.13, 4.14 and 4.15. This noise can often be compensated for or filtered.

Table 4.2 shows the wavelengths of the gratings before manufacture ( $\lambda_0$ ), after production ( $\lambda_p$ ), and after a period of installation ( $\lambda_1$ ) in the freeway. Although the wavelengths had moved slightly from the manufactured setting, each of the long gage configurations was still held in tension as of the writing of this report.

The relative height of the peaks corresponding to individual axles tended to vary more in the composite beam sensors. Although this may not be an ideal lead into WIM applications, it is logical that the sensitivity may be a function of several factors. It is anticipated that these variations may be corrected by understanding more about the sensor position in the roadway, tire position, embedment techniques, and sensor types, as applied to WIM. For vehicle axle counting or classification, these issues are of less concern.

**Table 4.2: Wavelengths (in nm) of each second-generation sensor**

Sensor	( $\lambda_0$ )	( $\lambda_p$ )	( $\lambda_1$ )
Sensor 5 (LGC)	1297.35	1299.55	1298.94
Sensor 6 (LGE)	1297.35	1299.5	1298.07
Sensor 7 (LGC)	1297.35	1299.09	1299.09
Sensor 8 (UNC)	1299.38	1299.38	1299.29



## 5.0 INTERFACING THE FIBER OPTIC TRAFFIC SENSORS FOR VEHICLE CLASSIFICATION

The FBG traffic sensor needs to be compatible with commercially available traffic recorders to be a viably useful sensor. But during this study, the sensor was not connected to a traffic recorder. Instead, it was interfaced directly to a demodulator system and selected signal traces were stored digitally on a computer.

To test its compatibility, the stored data were converted to a scaled analog voltage signal and fed directly into the piezoelectric inputs of a Diamond Traffic Product's Phoenix traffic classifier. The signal was software-adjusted to match the classifiers amplitude-triggering requirements. The output data are shown in Table 5.1 and are typical of standard classification information obtained by traffic counters. A number of various axle vehicles are represented, with the majority of traffic comprised of passenger cars.



Figure 5.1: The vehicle classifier box used to interface to the fiber optic sensors

**Table 5.1: Standard data output by the Diamond Phoenix Traffic Classifier interfaced with FBG traffic sensors**

Speed (Tenth's of ft/s)	MPH	# of Axles	Axle Length (ft)	Axle BIN #'s	Speed BIN #'s	Length BIN #'s	Gap BIN #'s	Headway BIN #'s	Spacings					
									1-2	2-3	3-4	4-5	5-6	6-7
798	54.4	3	20.2'	6	7	5	2	2	15.7'	4.5'	[13]	0		
929	63.3	2	10.9'	3	9	3	8	8	10.9'	[14]	0			
850	58.0	5	42.1'	9	8	8	8	8	11.1'	4.4'	22.4'	4.2'	[11]	0
946	64.5	2	11.7'	3	9	3	8	8	11.7'	[14]	0			
960	65.5	2	8.9'	2	9	2	7	7	8.9'	[14]	0			
994	67.8	2	11.6'	3	10	3	8	8	11.6'	[14]	0			
880	60.0	2	10.2'	2	8	3	8	8	10.2'	[14]	0			
910	62.0	5	54'	9	9	9	8	8	15.5'	4.4'	30.4'	3.7'	[11]	0
921	62.8	2	8.7'	2	9	2	8	8	8.7'	[14]	0			
1085	74.0	2	10.2'	2	11	3	8	8	10.2'	[14]	0			



## 6.0 A LOOK AT REMNANTS OF AN ORIGINAL TRAFFIC SENSOR

On August 20, 2002, Sensor 3 from the original installation was extracted for examination. The sensor had previously detached internally and had no response.

A saw cut was made along one side of the sealant and attempts were made to detach the sealant and sensor. The adhesion to the PCC was strong, preventing removal. A second saw cut was made on the other side, and the sealant/sensor was successfully removed after loosening the underside at the sealant's interface with the PCC. The sensor and a portion of its lead were then extracted as a unit. The pictures below highlight some of the discoveries.

Figure 6.1 shows the cut PCC, sealant and extracted fiber optic sensor with the sensor lead extended.



Figure 6.1: A sensor lead extends from an extracted fiber optic sensor

Figure 6.2 shows that a 1 cm (0.4 in) break in the tubing was found as the sensor runs along the bottom of the channel. Note that only the tubing and not the fiber optic is broken at this point. Attempts to recreate this type of break in the laboratory using combinations of heat and large forces were unsuccessful. Due to the exposure of the tubing at the interface between the sealant and the PCC, a possible cause of this break may have been from forces exerted by a crow bar while loosening the interface for extraction. The rest of the tubing appears normal; thus the large amounts of strain were found in a very localized area.



Figure 6.2: Over-capacity local strain forces most likely caused this tubing to stretch apart, as found at the bottom of the saw cut

Figure 6.3 shows that the adhesion between the hot bituminous sealant and the traffic sensor was not optimal. At some point during or after installation, the tubing and bulkhead were forcefully separated. A possible explanation was that a 3 cm (1.2 in) pocket of air formed around the bulkhead/tubing interface which did not allow the sealant to properly adhere. When the forces of traffic were added, a lack of sealant may have caused the pressures from the vehicles to non-uniformly strain this interface and pull it apart.



Figure 6.3: A 3 cm air pocket formed around this interface on the active sensing portion of the sensor



Figure 6.4: An arched sensor configuration is seen in this portion of the extraction

Figure 6.4 shows an approximate 1 in (25 mm) tall by 9 in (230 mm) long arch that formed in the course of installation. During the original installation, workers placed sealant on each end of the traffic sensor (over each bulkhead) and then filled in over the sensor with layers of sealant. The arch that formed may be attributed to the sensor not lying completely flat during roadway insertion, or may be due to air bubbles causing the light sensor tubing to float upward. An arch of this magnitude may have increased the friction present and response capability of the fiber grating inside, causing the fiber line to break.



## 7.0 CONCLUSIONS

The second-generation sensor installation proved to be valuable for learning more about fiber optic grating traffic sensors, from the standpoint of experimental data collected. Although the data appear to show that a composite beam approach reduced the recovery time of the sensor, an advantage, from a design standpoint, is that the sensor was less susceptible to sudden shock or overstrain. Another success is that the enhanced version of the original sensor functioned as designed, without detaching from the housing. It also appeared to function fairly well as a vehicle classification sensor.

Using the vehicle classification unit, data was interpreted by the classifier after first being amplitude adjusted through software-controlled filtering. Although this method was successful after some effort, future designs of demodulation hardware could incorporate this modification through electronic means.

In early 2003, costs for the initial traffic sensors ranged from \$600-\$700. It is expected that volume quantities of thousands would drop the price an order of magnitude.

For the data acquisition and electronics to convert the optical signal to an electrical voltage compatible with vehicle classifier boxes, a unit was loaned by Blue Road Research. Current cost is several thousands of dollars. It is anticipated that this cost would also drop to \$1K-\$2K in large volumes of thousands.



## 8.0 EVALUATION AND RECOMMENDATIONS

The results of this research have shown the feasibility of using fiber grating strain sensors to monitor heavy traffic on PCC roads. The sensitivity of the system is sufficiently high that adjacent lane traffic can also be detected, opening up new possibilities of monitoring several lanes of traffic from one location. Monitoring traffic from the shoulder area is also appealing by providing a safer installation, less traffic disruption and lower stress on the sensor. Such a system could be versatile and cost efficient.

For this study, all sensors were installed in only one wheel path to aid in the understanding and evaluation of the prototype sensors. This approach is feasible for vehicle classification and counting needs and can be accomplished using two sensors at a known spacing [e.g. 7 ft (2 m)]. For WIM uses, an approach would be to install one sensor in each wheel path, staggered 7 ft (2 m) apart, to capture speeds as well as weights of both sides of the vehicle.

To support WIM, it will be necessary to modify the design of the sensors and their placement so that the position of the wheel on the fiber grating sensors does not affect the measurement. This might be achieved using displaced sets of fiber grating strain sensors to determine lane position. Because the hot bituminous sealant used would likely change properties with temperature, it would be necessary to perform calibration periodically until baselines for temperature have been established in the WIM application. Wear of the road may also change the response, which in turn would require periodic calibration. Since the fiber grating sensors have shown high sensitivity when buried at a depth of 3 in (76 mm), it should be possible to resurface the road without damaging the fiber grating sensors. The repair procedures used could significantly alter response. As a minimum, it appears feasible for the fiber grating sensor to operate successfully for years without replacement.

Thus far, data shows that the fiber grating traffic sensor has the potential to be a long-lasting, cost-effective solution for vehicle classification and WIM applications.



## 9.0 FUTURE WORK

Because of the potential capability of this device for WIM use, further investigation of FBG traffic sensors for WIM is recommended. Future work may include modifying and improving the second-generation fiber grating strain sensors and packaging to analyze capabilities for WIM by studying same-vehicle repeatability, vehicle calibration, and axle response/stability. A further effort with interface requirements should also occur; as an optimal interface for retrofitting with existing equipment would be hardware-convertible and not require the use of a computer.

To advance this technology for WIM capabilities, these sensors should be further characterized to determine any position-dependant effects related to tire(s) crossing over the sensor. This can be done by offsetting sensors in the roadway to determine tire position. Further, a study of the optimal installation depth, speed-related effects, and materials and procedures for installation should be examined. As this is a leading-edge technology, no database or library of information exists to determine how these factors influence measurement data.

Potential uses of this technology in WIM applications may include improved ability to monitor or enforce existing traffic and weight limits along roadways and bridges, which could increase the lifespan of these structures and enhance roadway safety.



## 10.0 REFERENCES

- Lai, Leon L., "Weigh-in-motion and Smart Bridges", International Society for Optical Engineering, SPIE Vol. 3043, p. 23-30, May 1997.
- Meller, Scott A., Marten J. de Vries, Vivek Arya, Richard O. Claus, Noel Zabaronick, "Advances in Optical Fiber Sensors for Vehicle Detection, International Society for Optical Engineering, SPIE Vol. 3207, p. 318-322, January 1998.
- Schulz, Whitten L.; John M. Seim, Eric Udd, Mike Morrell; Harold M. Laylor, Galen E. McGill, Robert Edgar, "Traffic Monitoring/Control and Road Condition Monitoring using Fiber Optic-based Systems", International Society for Optical Engineering, SPIE Vol. 3671, p. 109-117, May 1999.
- Schulz, W.L., E. Udd, J.M. Seim, G.E. McGill, "Advanced Fiber-Grating Strain Sensor Systems for Bridges, Structures, and Highways", International Society for Optical Engineering, SPIE Proceedings, Vol. 3325, p. 212, June 1998.
- Seim, J., E. Udd, W. Schulz, H.M. Laylor, "Composite Strengthening and Instrumentation of the Horsetail Falls Bridge with Long Gauge Length Fiber Bragg Grating Strain Sensors", OFS-13 Symposium, Kyongju, Korea. April 1999(a).
- Seim, J., E. Udd, W.L. Schulz, M. Morrell, H.M. Laylor, "Health Monitoring of an Oregon Historical Bridge with Fiber Grating Strain Sensors", International Society for Optical Engineering, SPIE Proceedings, Vol. 3671, p. 128, May 1999(b).
- Teral, Stephanie R., "Fiber Optic Weigh In Motion: Looking Back and Ahead", International Society for Optical Engineering, SPIE Vol. 3326, p. 129-137, June 1998.
- Udd, E., J. Seim, W. Schulz, R. McMahon, S. Soltesz and M. Laylor, "Monitoring Trucks, Cars, and Joggers on the Horsetail Falls Bridge Using Fiber Grating Strain Sensors", International Society for Optical Engineering, Proceedings of SPIE, Vol. 4185, p. 872, December 2000.